Soil Dynamics and Earthquake Engineering 124 (2019) 230–258

Contents lists available at ScienceDirect

Soil Dynamics and Earthquake Engineering

journal homepage: www.elsevier.com/locate/soildyn

Multidirectional cyclic shearing of clays and sands: Evaluation of two bounding surface plasticity models

Ming Yang, Gaziz Seidalinov, Mahdi Taiebat*

Department of Civil Engineering, University of British Columbia, Vancouver, BC, Canada

ARTICLE INFO

Keywords:
Multidirectional cyclic shearing
Constitutive models
Clay
Sand
SANICLAY
SANISAND

ABSTRACT

Seismic site response analysis (SSRA) is typically performed considering only one horizontal component of earthquake excitation. In many cases, however, two or three components are needed for the analysis to properly account for the true multidirectional nature of seismic loading. In this type of analysis, it is essential to use multiaxial constitutive models that can realistically describe the stress-strain response of soils. Development and validation of such constitutive models are essential steps toward this goal. Fortunately, a large quantity of experimental data from multidirectional cyclic shear tests is available and can provide physical basis for validating such models. This paper focuses on evaluation of two members of the SANICLAY and SANISAND families of constitutive models for simulating the response of clay and sand, respectively, when subjected to multidirectional cyclic shearing. The models have anisotropic elasto-plastic formulation, within the framework of critical state soil mechanics, and follow the bounding surface plasticity theory. They are calibrated and evaluated against experimental data on Gulf of Mexico clay and Monterey No. 0/30 sand in undrained multidirectional cyclic shear tests, including linear, circular/oval, and figure-8 loading paths. This study provides a basis for evaluation of the capabilities of these models in multidirectional shearing, thereby paving the way towards future applications in multidirectional SSRA.

1. Introduction

In recent decades, the destructive nature of earthquakes on constructed facilities has led to extensive research focused on the dynamic properties of soil. Direct simple shear (DSS) test has been chosen as a close configuration to model the plane strain condition and the rotation of principal stress axes in soil [1]. In this test, during the cyclic regime only one horizontal shear component is exerted on the specimen. With or without an offset static shear stress in the same direction as the cyclic shear stress, this unidirectional shear mode can be used to replicate the response of soil subjected to one-dimensional propagation of shear waves. In the field, however, shear wave propagation is multidirectional. Even if the vertical component of the seismic loading is neglected, there exist two horizontal shear components as depicted in Fig. 1(a), and neglecting one of them can potentially lead to underestimation of seismic demand. To mimic the response of soil element under level or sloping grounds, when subjected to multidirectional cyclic shearing, a number of more sophisticated devices for simulating the multidirectional cyclic shearing have been established, developed and refined over the years [2,1,3–7]. These apparatuses are very useful in generating a comprehensive experimental database for evaluation of various constitutive models in such complex loadings.

The soil sample in a multidirectional cyclic shear test goes through two loading stages. The first one, referred to as consolidation stage, is to reproduce the corresponding in situ state of soil cconsolidated under level or sloping grounds as shown in Fig. 1(a). For modeling the initial condition of soil under a level ground (away from a slope), a soil element is consolidated vertically with the lateral normal strains constrained; this is typically referred to as K_0 condition. For the soil element under the sloping ground, in addition to the above normal consolidation, an offset consolidation shear stress τ_c perpendicular to the strike direction of the slope is also exerted on the element, as depicted in Fig. 1(b) with blue dashed arrow; this is referred to as anisotropic consolidation and denoted as K_α condition. Here $\alpha = \tau_c/\sigma'_{vc}$ is the normalized magnitude of the offset consolidation shear stress, i.e., the ratio of τ_c and initial effective vertical stress σ'_{vc} applied on the top plane of the element. A good equivalent interpretation of the ratio α is static stress ratio (SSR) [8], analogous to the widely-used notation cyclic stress ratio (CSR) used to represent the normalized magnitude of cyclic shearing. It should be noted that this K_α only

* Corresponding author.
E-mail address: mtaiebat@civil.ubc.ca (M. Taiebat).

https://doi.org/10.1016/j.soildyn.2018.05.012
Received 26 October 2017; Received in revised form 29 April 2018; Accepted 8 May 2018
Available online 27 June 2018

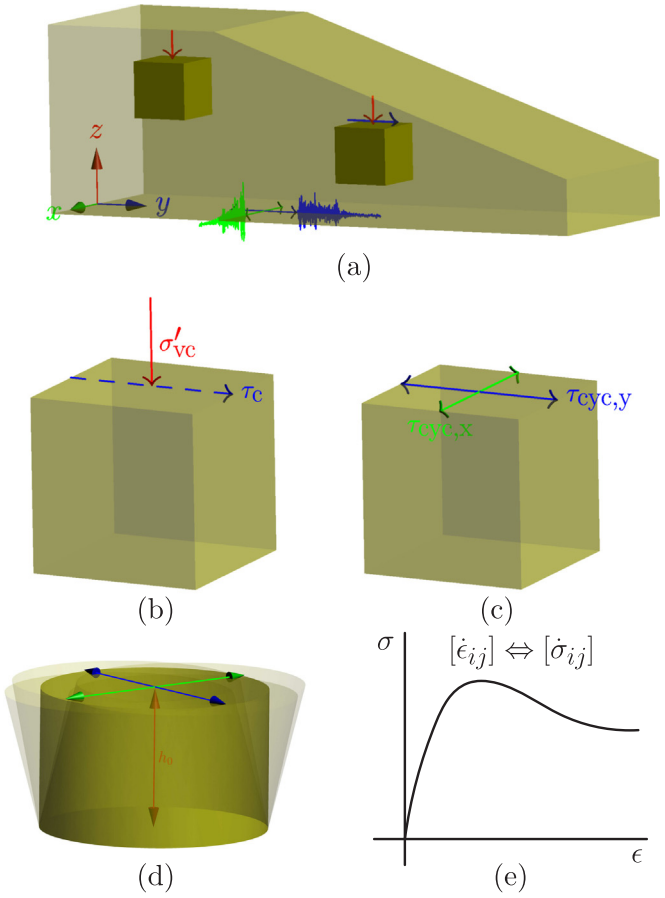

Fig. 1. Multidirectional properties of seismic loading in real field: (a) seismic loading, (b) consolidation stage, (c) cyclic shearing stage, (d) element in experimental tests, and (e) stress-strain relationship.

defines the aforementioned anisotropic consolidation condition, different from the well-known K_α correction used in liquefaction triggering analysis. A simpler case of initial condition for the first loading stage, but perhaps less realistic in the nature, is isotropic consolidation of the sample set-ups of Ishihara and Yamazaki [2] and Ishihara and Nagase [9]. Accounting for all these possibilities in laboratory tests, there are three kinds of consolidation stages depending on whether the specimen is consolidated under isotropic, K_0 or K_α conditions, and these conditions are denoted by CI, CK_0 and CK_α, respectively. Among these stages, only CK_α would result in non-zero SSR.

The second loading stage is referred to as cyclic shearing stage. During seismic excitation on level or sloping grounds, the vertically propagating shear waves within the soil profile induce irregular dynamic shearing in soil. This irregular shear loading may be simplified by introducing an equivalent time history of harmonic shearing, denoted by $\tau_{cyc}(t)$. Similar to the irregular dynamic loading, $\tau_{cyc}(t)$ can change in both magnitude and orientation. With the coordinate system shown in Fig. 1(a), i.e., the x-axis along the strike direction of the slope, the y-axis perpendicular to that and along the slope projection on the horizontal plane, and the z-axis being vertical, the $\tau_{cyc}(t)$ can be resolved into two orthogonal components, $\tau_{cyc,x}$ and $\tau_{cyc,y}$, as depicted in Fig. 1(c). After the initial consolidation stage shown in Fig. 1(b), the cyclic shear paths from the two orthogonal cyclic shear components are to be applied in the element test as shown in Fig. 1(c). It should be noted that for this stage of element test, a stress controlled input is used in most of the available multidirectional cyclic shear tests, except the ones by Matsuda et al. [4,10–12], and Nhan and Matsuda [13] where the input path is strain controlled.

Majority of the laboratory element tests are performed under either drained or undrained conditions. The rapid nature of seismic excitation does not allow enough time for dissipation of pore pressure in the in situ state of soil, thereby requiring that laboratory tests be performed under undrained conditions to mimic the idealized field condition. To the authors' knowledge, almost all the multidirectional cyclic shear tests in the literature are carried out in undrained condition. Assuming a fully saturated condition and a nearly incompressible response for both water and solid grains of soil, to model the undrained condition the volume of the specimen should be kept constant during the cyclic shearing stage. With the lateral normal strains constrained, a constant volume condition can be achieved either by keeping the height of the dry specimen (h_0) constant ("constant height" test) or by closing the drainage valve of the saturated specimen ("truly undrained" test). The former manner is very common in DSS testing where the top face of the specimen is only allowed to deform along one shear direction while the latter one is adopted in the multidirectional cyclic shearing test where the top face can move with variable shear directions as shown in Fig. 1(d) with shadows referring to the deforming directions. More details about the equivalence of the "constant height" and "truly undrained" DSS tests are presented in [14]. Note that the state reflected in Fig. 1(d) should be referred to as "multidirectional cyclic shear" instead of "multidirectional cyclic simple shear" as sometimes seen in the literature, because the typical adjective "simple" implies plane strain condition, which does not apply to the multidirectional cyclic shearing [15]. There are known concerns and limitations common between the DSS and the multidirectional cyclic shear test, mainly related to the non-uniformity of stresses and strains, and equalization of pore pressures. One should keep in mind these limitations when judging the results obtained from these tests.

A number of requirements have to be met in a constitutive model for its application in the simulation of multidirectional cyclic shear response of soils. The most basic one is having the constitutive model formulated in the multiaxial space based on proper tensorial formulation. This is because this type of loading involves variations of both magnitude and orientation of the principal stress components, and therefore simplistic constitutive models such as those formulated for plane strain condition would not be applicable. Other important requirements needed for proper modeling of any cyclic loading in soils, are proper mechanisms for reproducing the soil stiffness and strength, coupling between the volumetric and deviatoric responses, and addressing the changes of soil stiffness in the unloading and reloading sequences.

The next sections are focused on the evaluation of two advanced plasticity models in simulating multidirectional cyclic shear test. These are members of the Simple ANIsotropic CLAY and SAND families of plasticity models, which are more briefly referred to as SANICLAY and SANISAND, respectively. First, an overall experimental database of the multidirectional cyclic shear tests available in the literature are summarized and presented in Section 2. Then details about the selected experiments to be simulated in this paper are presented in two tables. In Section 3, background and highlights of the two selected bounding surface constitutive models for modeling the cyclic response of clay and sand are presented along with discussion on their similarities and differences. Calibrations of the models are presented in Section 4 based on some monotonic and simple cyclic tests, which indicates the capabilities of these two models in capturing the stress-strain behavior of clay and sand subjected to conventional loading conditions. In Section 5, the corresponding model simulations for the multidirectional cyclic shear tests are presented and compared with the experimental results. Discussion about the performance of the models in the so called neutral loading paths, very common in majority of classical

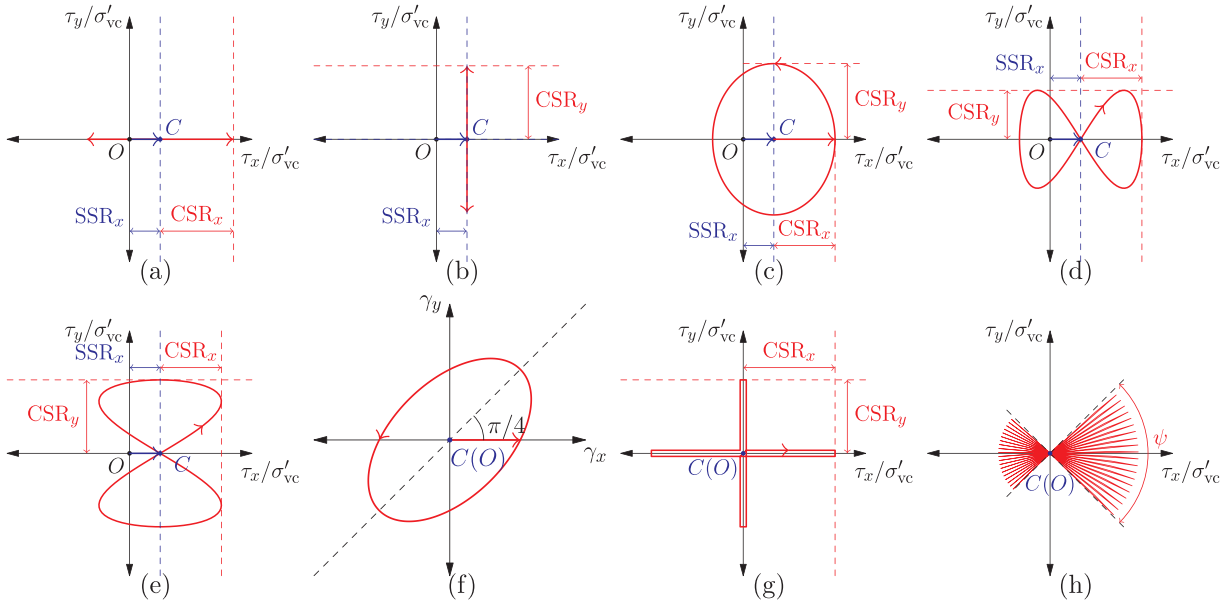

Fig. 2. Cyclic shearing paths summarized in Yang et al. [15] during cyclic shearing stage: (a) 1-D linear path, (b) 2-D linear path, (c) circular/oval path, (d) figure-8 type A path, (e) figure-8 type B path, (f) rotated oval path, (g) alternate path, and (h) sector path.

Table 1
Experimental database for multidirectional cyclic shear tests on clays and sands.

Shearing path	Initial state	Material	Source
1-D linear path	CK_α	Gulf of Mexico clay	Rutherford [18]
2-D linear path	CK_α	Gulf of Mexico clay	Rutherford [18]
Circular/oval path	CK_0	Gulf of Mexico clay	Rutherford [18]
	CK_α	Gulf of Mexico clay	Rutherford [18]
Figure-8 type A path	CK_0	Gulf of Mexico clay	Rutherford [18]
	CK_α	Gulf of Mexico clay	Rutherford [18]
Figure-8 type B path	CK_0	Gulf of Mexico clay	Rutherford [18]
	CK_α	Gulf of Mexico clay	Rutherford [18]
Rotated oval path	CK_0	Kaolinite clay	Matsuda et al. [12], Nhan and Matsuda [13]
		Tokyo bay clay	Matsuda et al. [12], Nhan and Matsuda [13]
		Kitakyushu clay	Matsuda et al. [12], Nhan and Matsuda [13]
Sector path	CK_0	Soft clay	Nie et al. [19]
1-D linear path	CK_α	Sacramento River sand	Boulanger et al. [16]
		Monterey No. 0/30 sand	Kammerer et al. [17]
2-D linear path	CK_α	Sacramento River sand	Boulanger et al. [16]
		Monterey No. 0/30 sand	Kammerer et al. [17]
Circular/oval path	CI	Fuji River sand	Ishihara and Yamazaki [2]
	CK_0	Monterey No. 0/30 sand	Kammerer et al. [17]
	CK_α	Monterey No. 0/30 sand	Kammerer et al. [17]
Figure-8 type A path	CK_0	Monterey No. 0/30 sand	Kammerer et al. [17]
	CK_α	Monterey No. 0/30 sand	Kammerer et al. [17]
Figure-8 type B path	CK_0	Monterey No. 0/30 sand	Kammerer et al. [17]
	CK_α	Monterey No. 0/30 sand	Kammerer et al. [17]
Rotated oval path	CK_0	Toyoura sand	Matsuda et al. [10,4]
		GBFS	Matsuda et al. [10,4]
Alternate path	CI	Fuji River sand	Ishihara and Yamazaki [2]
Sector path	CK_0	North Sea sand	Rudolph et al. [7]
Irregular path	CI	Fuji River sand	Ishihara and Nagase [9]

elastoplasticity models, is presented at the end.

2. Multidirectional cyclic testing data

2.1. Available experimental database

Based on the offset shear applied during the consolidation stage of the multidirectional cyclic shear test in combination with the amplitudes, frequencies, and phase angle differences of the two harmonic cyclic shear components applied during the shearing stage, different types of shearing paths can be generated from this test. Eight types of such multidirectional cyclic shear tests, all available in the literature, are presented in the space of the shear components of stress or strain in Fig. 2. In this figure, point *O* represents zero shear stress or strain states prior to the initial consolidation stage. Point *C* along the *x*-direction shows the state of the sample after the CI, CK_0, or CK_α consolidation stage, represented in blue; at this stage the normalized magnitude of the offset consolidation shear stress is given in terms of static stress ratio, SSR_x. Various undrained cyclic shear stress or strain paths are presented in red, for which the normalized magnitudes of the cyclic shear stresses along the *x* and *y* directions are given in terms of cyclic stress ratios, CSR_x and CSR_y. Yang et al. [15] have elaborated how these shearing

paths can be produced based on the mathematical expressions of the two shear components in the top plane of the sample. Some general information about the related available tests in the literature on clays and sands are summarized in Table 1.

The 1-D linear path, as shown in Fig. 2(a), is the traditional unidirectional cyclic shear test (commonly known as DSS), which may also include an initial offset shear stress in the same direction as the subsequent undrained cyclic shearing. This type of tests has been conducted by many researchers on different types of soil, and there is a wealth of data available on that [e.g., [16–18], as presented in Table 1]. When the undrained cyclic shearing is applied perpendicular to the direction of initial offset shear stress, the shearing path is denoted by 2-D linear path, as shown in Fig. 2(b). This type of shearing dates back to Boulanger et al. [16] on Sacramento River sand and later was adopted by Kammerer et al. [17] on Monterey No. 0/30 sand and Rutherford [18] on Gulf of Mexico clay.

Circular/oval path in Fig. 2(c) is first reported by Ishihara and Yamazaki [2] on Fuji River sand sample under CI condition. Later, such path was applied on Monterey No. 0/30 sand [17] and Gulf of Mexico clay [18] under CK_0 and CK_α conditions. Figure-8 type A and figure-8 type-B are two non-trivial shearing paths, as shown in Figs. 2(d) and (e), respectively. They are first reported in the experiments on Monterey No. 0/30 sand [17] and then on Gulf of Mexico clay [18]. Fig. 2(f) shows another non-trivial path named rotated oval as used by Matsuda et al. [4,10–12], and Nhan and Matsuda [13] on a number of clays and sands. Experiments with the so-called alternate path shown in Fig. 2(g) are reported by Ishihara and Yamazaki [2] on Fuji River sand under CI condition. Finally Fig. 2(h) presents a case where only the orientation of the planar shear stress magnitude continuously changes. This type of shearing has been adopted on North Sea sand [7] and a soft clay [19], with both cases being under CK_0 condition.

Aside from these, Ishihara and Nagase [9] have reported applying the reproduced shearing paths from real earthquakes on Fuji River sand specimen under CI condition, as listed in Table 1. There are also some other complex paths such as half-circular/oval path and cropped figure-8 path in [17], which for brevity are not illustrated in Fig. 2 or listed in Table 1.

2.2. Experimental tests for this study

From the described types of shearing paths, Table 1 includes two relatively rich groups of multidirectional cyclic shear tests on clay and sand: the tests on Gulf of Mexico clay by Rutherford [18], and the ones on Monterey No. 0/30 sand by Kammerer et al. [17]. Considering their details, these two groups of laboratory tests appear to be suitable for the performance evaluation of various constitutive models for multidirectional cyclic shearing of clay and sand. Particularly the sand database has been shared publicly by the authors where they provide all the experimental data online, from which such an evaluation study benefits extensively.

Table 2
Simulated experimental tests on Gulf of Mexico clay.

Test type	Test #	e^*_{in}	Consolidation stage			Shearing stage		
			$\sigma_{vc'}$[kPa]	SSR_x	SSR_y	CSR_x	CSR_y	N
1-D linear	GOM-5	2.230	83.60	0.000	0.000	0.200	0.000	90
	GOM-6	2.230	83.60	0.200	0.000	0.200	0.000	5
	GOM-7	2.230	83.60	0.200	0.000	0.150	0.000	26
2-D linear	GOM-8	2.230	83.60	0.200	0.000	0.000	0.200	14
Circular/oval	GOM-10	2.230	83.60	0.000	0.000	0.200	0.200	13
	GOM-11	2.230	83.60	0.200	− 0.060	0.200	0.200	7
	GOM-12	2.230	83.60	0.200	− 0.030	0.150	0.150	28
Figure-8 Type A	GOM-13	2.230	83.60	0.000	− 0.040	0.200	0.200	12
	GOM-14	2.230	83.60	0.200	0.000	0.200	0.200	3
	GOM-15	2.230	83.60	0.200	0.000	0.150	0.150	11

*e_{in} is the void ratio prior to the initial consolidation stage.

Table 3
Simulated experimental tests on Monterey No. 0/30 sand.

Test type	Test #	e^*_{in}	Consolidation stage			Shearing stage		
			$\sigma_{vc'}$[kPa]	SSR_x	SSR_y	CSR_x	CSR_y	N
1-D linear	ms66cyck	0.617	73.24	0.290	0.000	0.510	0.000	10
	ms67cyck	0.579	77.65	0.150	0.000	0.480	0.000	10
2-D linear	ms20cyck	0.665	76.75	0.101	0.022	0.000	0.234	35
	ms61cyck	0.668	82.58	0.141	0.029	0.000	0.254	50
Circular/oval	ms44cyck	0.651	84.52	0.025	0.007	0.232	0.397	18
	ms35cyck	0.655	87.91	0.094	0.030	0.233	0.118	20
	ms59cyck	0.696	54.66	0.216	0.009	0.192	0.376	20
Figure-8 Type A	ms33cyck	0.692	84.67	0.016	0.008	0.240	0.118	14
	ms38cyck	0.668	88.11	0.086	0.024	0.227	0.118	15
	ms52cyck	0.661	75.30	0.472	− 0.017	0.490	0.244	25

*e_{in} is the void ratio prior to cyclic shearing stage.

Details of all of the multidirectional cyclic shear tests that are simulated in this study are listed in Tables 2 and 3 for clay and sand, respectively. To numerically replicate the initial state of each sample, at least the initial void ratio e_{in} and the initial stress state are required for each case. All of these tests are carried out under either CK_0 or CK_α condition. In the initial consolidation stage, as the soil specimen is consolidated with lateral normal strains constrained, the initial consolidation effective vertical stress is denoted by σ'_{vc} and the normalized magnitude of initial offset shear stress along the x-direction is denoted by SSR_x. In order to simulate the experiments more accurately, in some cases a small value of SSR_y is also considered as reported in Tables 2 and 3. For cyclic shearing stage, the quantities of CSR along the x and y directions, and the number of loading cycles are listed in the two tables.

3. Constitutive models

Constitutive models describing stress-strain response of geomaterials are predominantly developed based on the macroscopic observations made in typical laboratory element tests (e.g. triaxial or DSS tests). Some of these models are purely empirical, while others are developed on the basis of certain theoretical frameworks, such as elastoplasticity. Some models are quite simple and have only a few parameters, with clear physical meanings, and are easy to calibrate, while others are more sophisticated and have a relatively larger number of model parameters that require availability of detailed laboratory test data for the calibration. It should be noted that not all the parameters have to have a direct physical meaning, because after all they are "model parameters". Ideally, a model should have a balance between the simplicity of its formulation and the representativeness of the intended material response. The choice of a proper constitutive model in an application largely depends on the type of loading and the nature of the governing aspects of the response in the loading of interest.

Over the last three decades a number of classes of constitutive models have been developed for soils. Some have been developed mainly to address certain aspects of response in monotonic loading, and some others mainly target the response in cyclic loading. Some are developed considering only the simpler plane strain condition of loading, and some others include the complete tensorial nature of stresses and strains. These models have shown various levels of success in capturing the response of soils in typical plane strain or axisymmetric loading conditions such as those in the DSS or triaxial tests. However, studies on evaluation of the constitutive models in multidirectional cyclic loading are very rare. This is understandable because of the complex constitutive features needed for successful performance of a model in such loading conditions.

The models considered in this study are from two classes of anisotropic critical state bounding surface plasticity models, namely

SANICLAY and SANISAND, developed and improved over the years for capturing the response of clay and sand. A brief summary of the background and features of each class, and the versions used in the present study is presented in this section.

3.1. SANICLAY

SANICLAY is the name for a class of Simple ANIsotropic CLAY plasticity models. The class originates from the work of Dafalias [20] who proposed anisotropic extension of the Modified Cam-Clay (MCC) model by incorporating an anisotropic variable in the work dissipation equation, leading to a plastic potential function. The resulting plastic potential surface in the triaxial *p-q* space, which for associative plasticity serves also as a yield surface, is a rotated and distorted ellipse. Later, by using a non-associated flow rule, Dafalias et al. [21] extended the earlier work to allow the simulation of softening response under undrained compression following oedometric consolidation. This was when the name SANICLAY was first adopted for this class. Although the SANICLAY model was able to capture anisotropy as well as softening response in soft clays, it did not have enough means to capture the loss of structure in loading of natural sensitive clays. Taiebat et al. [22] proposed a versatile extension of the SANICLAY model by incorporating two distinct mechanisms for modeling of destructuration: isotropic and frictional. They also generalized the SANICLAY model itself from its previous form by additional dependence of the yield surface to a stress Lode angle. The formulation of the model and its structured generalization are structured in a modular way, so that some of its features can be turned off when not needed.

Up to this point, for stress changes inside the yield surface the SANICLAY models included only elastic deformations. Taiebat et al. [23] employed the bounding surface concept along with radial mapping rule in an efficient and practical version of the SANICLAY model with non-associated flow rule and destructuration in triaxial space, to permit plastic deformations for stress changes even within the yield surface (contrary to classical plasticity) and thereby to better simulate the stress-strain response under both monotonic and cyclic loading conditions. The work was improved by Seidalinov and Taiebat [24] who used an evolving projection center and a damage parameter for successful simulations of undrained cyclic triaxial tests and presented the model in full multiaxial formulation. They showed that updating projection center, used for projecting current stress onto the bounding surface thereby providing image stress required for adopted bounding surface formulation, is required for more realistic representation of clay stiffness in unloading and reloading stages. The damage parameter introduced in the model was shown to be beneficial for accumulating the plastic deviatoric strains with the number of cycles. This latest version of the model is used in the present study for modeling the response of clay, and is referred to with the generic name of SANICLAY hereafter.

Other extensions of the model include different yield surface shapes [25], different rotational hardening rules [26,27], and accounting for rate-dependency using Perzyna's overstress theory [28]. For simplicity these extensions are not considered in the present study as their focus has been essentially on monotonic loading.

Schematic diagram of the SANICLAY model in the principal stress space is shown in Fig. 3. The model consists of the bounding, critical state, and plastic potential surfaces as illustrated in this figure. The bounding surface, that replaces the traditional yield surface, can change in size (isotropic hardening), and rotate/distort (rotational hardening). The plastic potential defines the flow rule, i.e., coupling between plastic volumetric and deviatoric strain increments. It shares the same anisotropy line with the bounding surface and passes through the image stress. Out of these three surfaces, only the critical state and plastic potential surfaces are Lode angle dependent. The image stress is located using a radial mapping rule, projecting current stress from a projection center on the bounding surface. Projection center is updated at each stress reversal and evolves with the evolution of bounding surface in order to maintain its relative position within it.

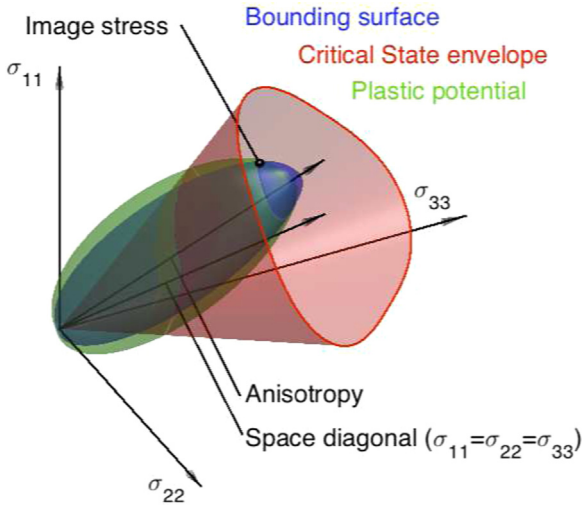

Fig. 3. Schematic diagram of the SANICLAY model in the principal stress space.

3.2. SANISAND

SANISAND is the name for a class of Simple Anisotropic SAND constitutive models. The class originates from a simple and elegant formulation of two-surface plasticity model developed by Manzari and Dafalias [29]. The modeling approach is based on the framework of critical state soil mechanics, and the bounding surface plasticity platform. The operation of the bounding surface takes place in the deviatoric stress-ratio space, and the state parameter of Been and Jefferies [30] is used to define the peak and dilatancy stress ratios, and to unify the description of response in a wide range of pressures and densities with the same set of model parameters. Using this concept and a small stress-ratio based yield surface, the model includes features such as hardening or softening, and tendency for dilation or contraction, that in undrained loading would result in variations of mean effective stress and pore water pressure. Based on the simple and attractive foundation of this model, various extensions have been developed over the years. These include accounting for evolving fabric dilatancy by Dafalias and Manzari [31], inherent fabric anisotropy by Dafalias et al. [32], plastic strain in constant stress-ratio loading by Taiebat and Dafalias [33] (where the name SANISAND was first adopted), anisotropic critical state theory by Li and Dafalias [34], and zero purely elastic domain by Dafalias and Taiebat [35]. The work by Manzari and Dafalias [29] represents the core of the constitutive model and the above-referenced subsequent works present additional constitutive ingredients. To involve fewer model parameters and for simplicity, the version of the SANISAND model with evolving fabric anisotropy by Dafalias and Manzari [31] is considered as the basic candidate for the numerical simulations in the present study, along with an overshooting correction scheme described by Dafalias and Taiebat [35], and is referred to with the generic name of SANISAND hereafter.

Schematic diagram of the selected SANISAND model in the principal stress space is shown in Fig. 4. In the stress space, the model consists of a narrow open Lode angle independent cone-type yield surface, and three concentric Lode angle dependent bounding, classical critical, and dilatancy surfaces as illustrated in this figure. The yield surface has a fixed opening size and is allowed to rotate in the stress space (rotational hardening), which underpins cyclic plasticity. For constant stress ratio paths, only elastic strains take place as stress state remains inside the yield surface. The bounding surface formulation mathematically guarantees a smooth transition from the purely elastic domain to the elastoplastic domain. The dilatancy surface shares the same idea with the phase transformation line in the laboratory findings, within and outside

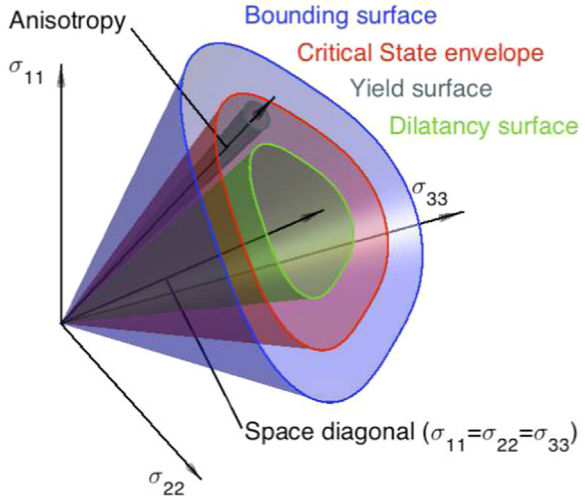

Fig. 4. Schematic diagram of the SANISAND model in the principal stress space.

which the response is contractive and dilative, respectively. The opening sizes of these latter surfaces are determined through the state parameter, with the critical state envelope acting as an attractor. For a state parameter of zero, both surfaces coincide with the critical state envelope.

3.3. Comparison

The selected versions of SANICLAY and SANISAND models similarly adopt the classical Lode angle dependent critical state theory, i.e., unique existence of critical state in the space of mean effective stress, p, and void ratio, e. The bounding surface formulation in both models relies on the stress reversals as an indication for initiation of new loading process enabling both of these models to mimic the change of stiffness in unloading and reloading events as observed in experiments. However, distance dependence of plastic modulus in their bounding surface formulation differs in the sense that SANICLAY uses measurement of Euclidean distance in the stress space, while SANISAND uses measurement in the stress ratio space. This is a result of a basic difference between clay and sand behaviors based on their simplified idealization; i.e. clays as assemblies of soft particles and sands as assemblies of hard particles. In clays, plasticity can take place for loading in any loading direction, i.e. either with changes of stress ratio or with constant stress ratio, while in sands plasticity usually takes place for changes of stress ratio, as long as particle crushing mechanism is not involved. Another substantial difference between these two models is the flow rule that determines plastic strain increments. In SANICLAY, the flow rule is explicitly defined by means of plastic potential whose gradient provides the direction of plastic strain increment and thereby the ratio between its volumetric and deviatoric counterparts. In SANISAND, however, there is no explicit definition of plastic potential; instead the dilatancy surface is used for defining the plastic volumetric strain increment, and a deviatoric non-associated flow rule is introduced for the plastic deviatoric strain increment in the stress ratio space. Specific features are present in SANICLAY and SANISAND models with some success for reproducing strain softening and cyclic liquefaction, respectively, as observed in the experiments. In SANICLAY, a scalar-valued damage parameter is used evolving with magnitude of plastic deviatoric strains. The damage parameter directly affects plastic modulus, and consequently plastic volumetric and deviatoric strain increments. In SANISAND, fabric dilatancy tensor is used evolving with the plastic volumetric strain increment with respect to the loading direction. The fabric dilatancy tensor directly affects the contraction tendency in reverse loading that follows dilation regime.

These two models have shown reasonable performance in reproducing some aspects of response in both monotonic and cyclic response of clays and sands, mainly in triaxial loading conditions [e.g., [31,21,36,22,24]]. The validation studies are however still limited, and need to be expanded to a broader range of loading conditions. With this background in mind, in the present study these models are calibrated and used for evaluation of their performance in a number of very complex multidirectional cyclic shearing scenarios with reference to the tests described in the previous section.

Table 4
Model parameters of SANICLAY for Gulf of Mexico clay.

Model parameters	Symbol	Value
Elasticity	κ	0.06
	ν	0.2
CSL	λ	0.247
	M_c	1.1
	M_e	0.81
Bounding surface	N	1.1
	h_0	80
	a_d	4
Rotational hardening	C	3
	x	1.75

4. Calibration of the models

The SANICLAY and SANISAND models are calibrated using experimental data of Gulf of Mexico clay [37,18] and Monterey sand [38,17], respectively. The calibration process in each case is briefly discussed in this section, with emphases on the parameters responsible for cyclic loading simulations. The parameters are calibrated essentially against a cyclic 1-D linear test (DSS) in each case, and then the calibrated models are used in the next section for simulations of various multidirectional cyclic shear tests in the corresponding database.

4.1. Gulf of Mexico clay

The Gulf of Mexico clay database used in this study is from a testing program at the University of Texas, Austin [18]. Detailed description of sampling and geotechnical characterization of the tested undisturbed samples is available in [38,17]. The deposits in the area from which samples were taken consist of uniform surficial highly plastic Holocene clays. Samples were retrieved from 30 different locations with varying degrees of seabed sloping. As the shallower samples were too soft, the testing program was performed on samples below 7 m depth. The plasticity index for these samples was in the range of 40–55, consisting of 51–72% of clay particles.

In addition to multidirectional cyclic shear tests, which are of direct interest in the present study, Rutherford [18] also conducted constant rate of strain consolidation tests of the samples, and using Casagrande's graphical method estimated a pre-consolidation stress of around 72 kPa. Murali [37] also conducted a series of undrained monotonic triaxial tests on these samples starting from either isotropic or K_0 consolidation states. Calibration of the model parameters is following the process described by Seidalinov and Taiebat [24], unless otherwise specified. The calibrated model parameters are presented in Table 4. The slopes of the normal consolidation and the rebound lines in the e–ln p space, denoted by λ and κ, respectively, are calibrated from the constant rate of strain consolidation tests. The experimental data is available in e–ln σ_a space and the procedure described by Taiebat et al. [22] is followed to transform the data into the e–ln p space. The critical state stress ratios M_c and M_e, corresponding to the triaxial compression and extension, respectively, are calibrated from undrained triaxial compression and extension tests on CK_0 specimens sheared from stress states corresponding to a range of OCR values. The stress ratio N at the apex of the bounding surface is calibrated from the stress path recorded for undrained triaxial compression test on CK_0 normally consolidated

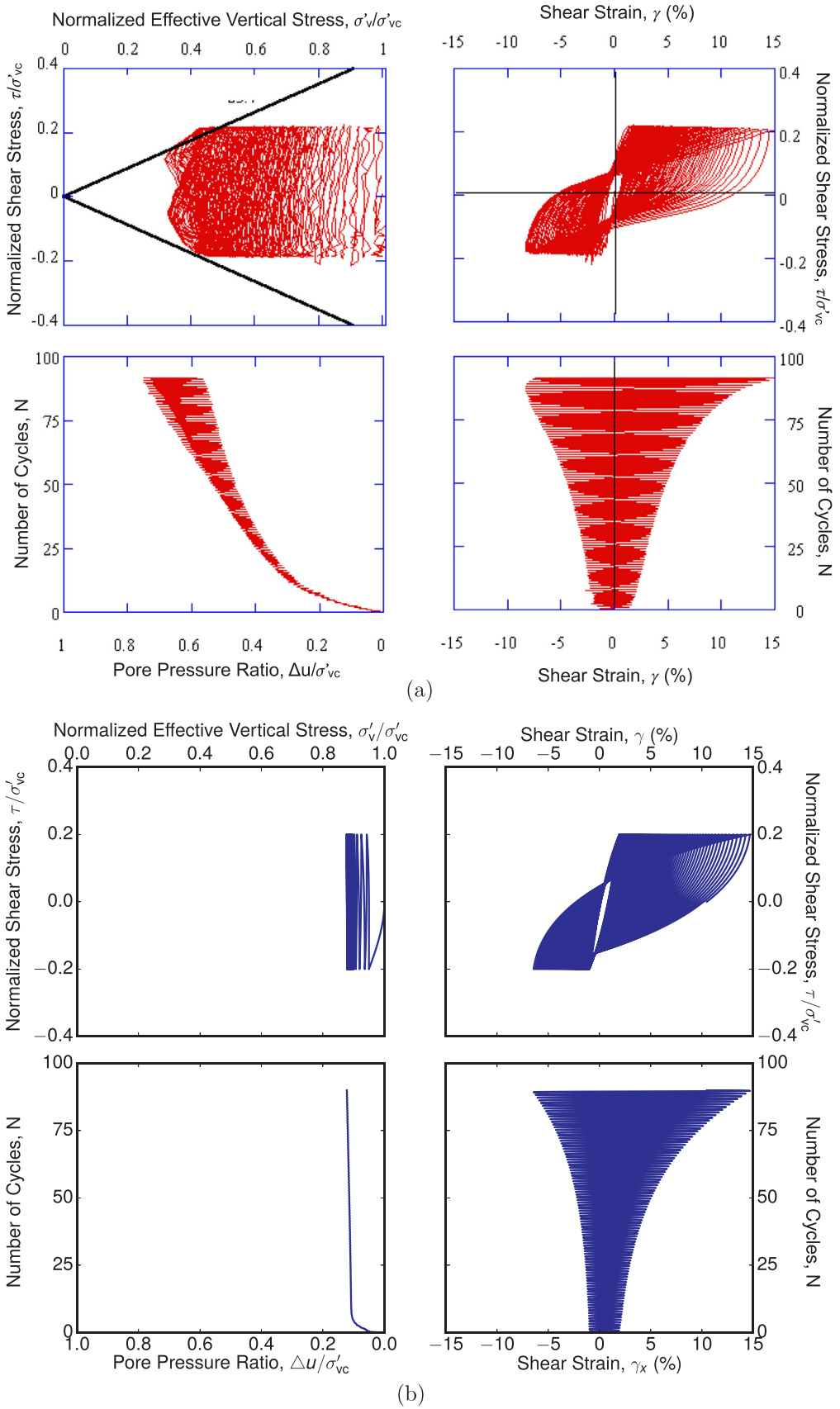

Fig. 5. Simulation versus experiment in undrained 1-D linear test GOM-5 on CK_0 consolidated sample of Gulf of Mexico clay: (a) experiment [18] and (b) simulation.

specimen. Due to unavailability of K_0-unloading, preceded by K_0-consolidation test, the Poisson's ratio $\nu = 0.2$ is assumed. The model parameter x, used for saturation of anisotropy during constant-η loading, is estimated using standard equation used in SANICLAY family models and K_0 value obtained using Jacky's equation with $\phi = 28°$ corresponding to the calibrated M_c and M_e values.

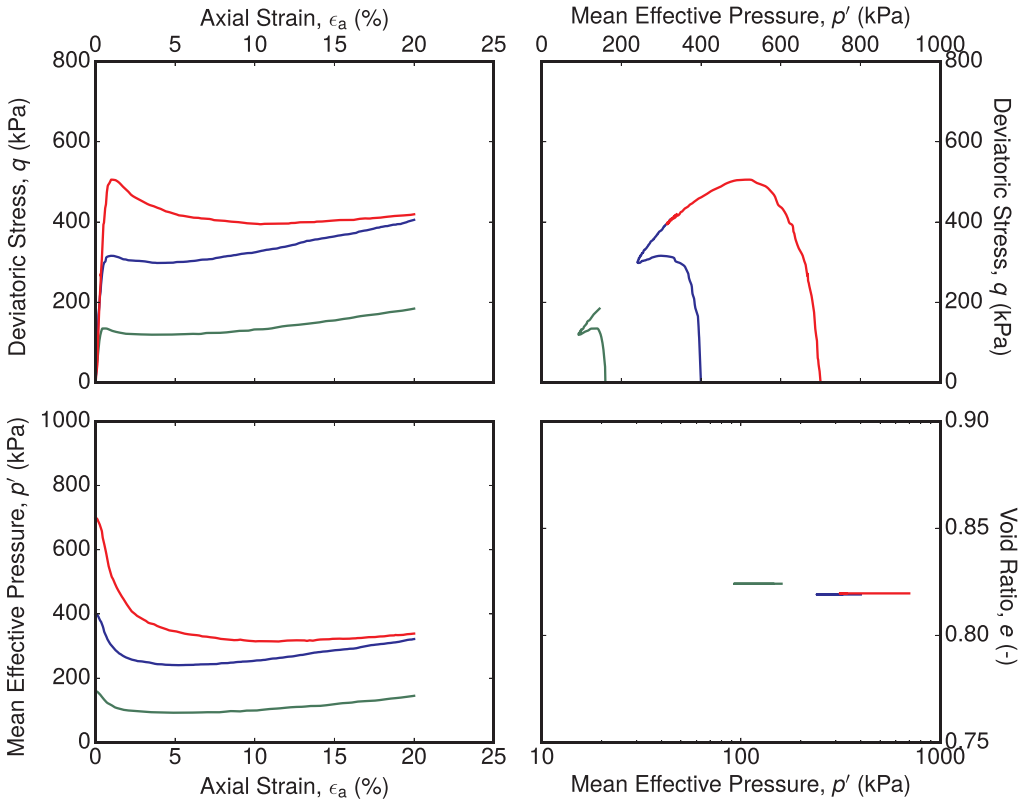

(a)

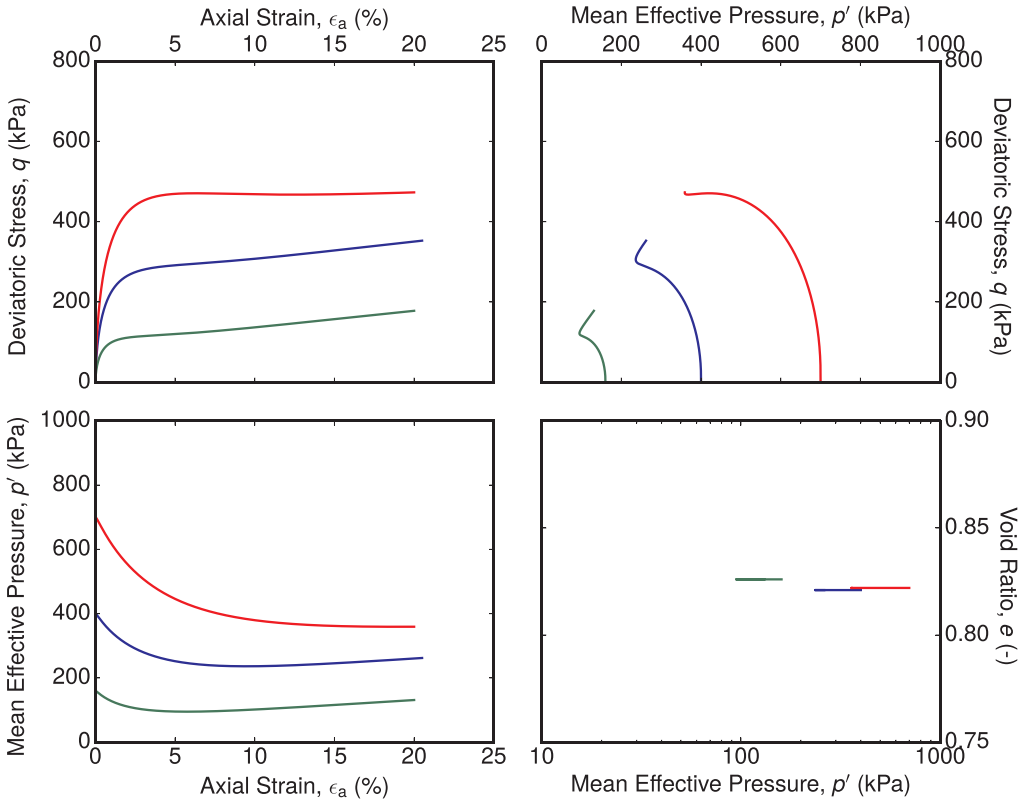

(b)

Fig. 6. Simulations vs experiments in undrained triaxial compression tests on isotropically consolidated samples of Monterey No. 0 sand: (a) experiments [42] and (b) simulations.

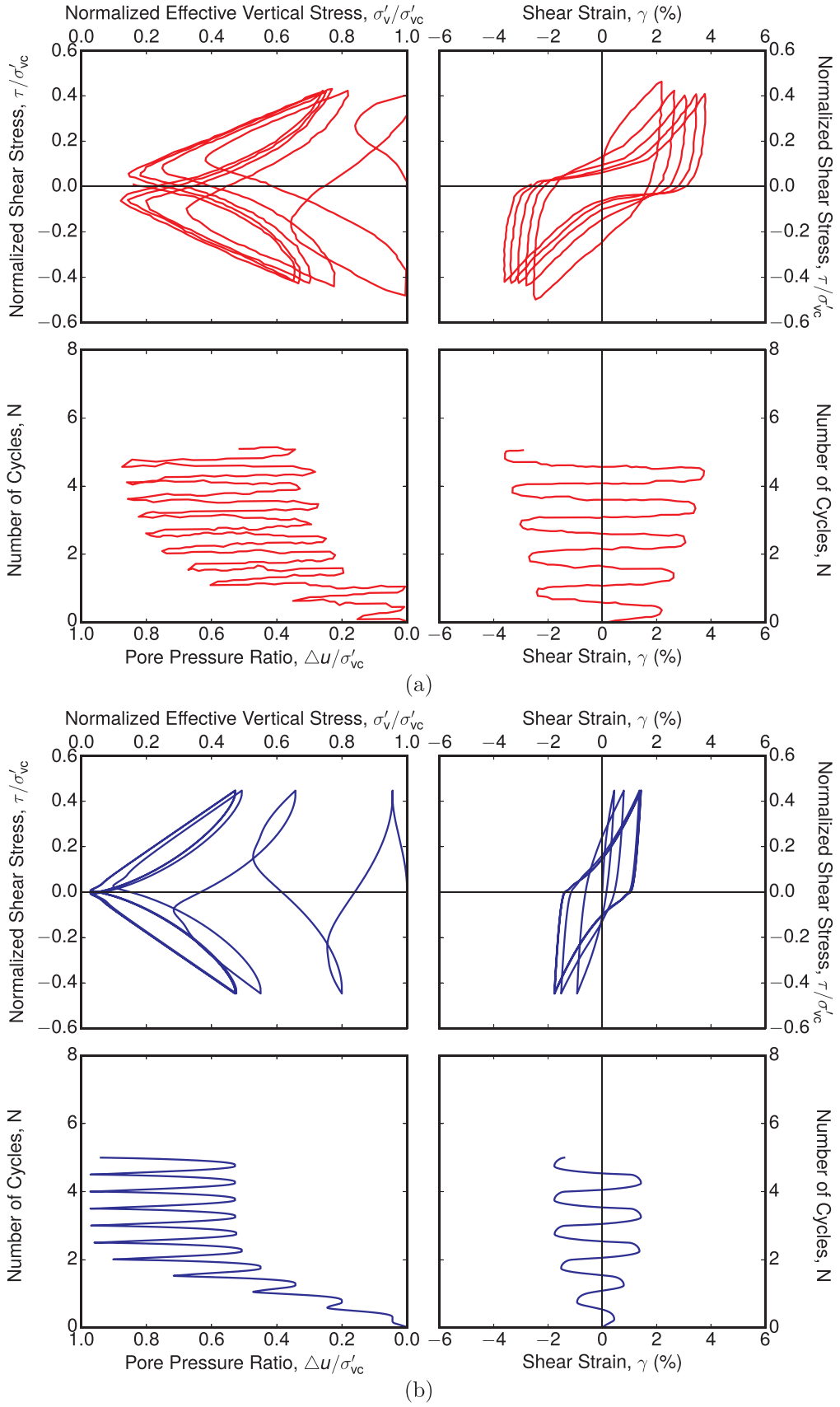

Fig. 7. Simulation vs experiment in undrained direct simple shear tests on CK_0 samples of Monterey No. 0/30 sand with D_r = 75%: (a) experiment [38] and (b) simulation.

Table 5
Model parameters of SANISAND for Monterey No.0/30 sand.

Model parameters	Symbol	Value
Elasticity	G_0	101
	ν	0.039
CSL	M	1.32
	c	0.718
	e_0	0.849
	λ	0.01
	ξ	0.7
Yield surface	m	0.03
Dilatancy	n^d	2.0
	A_0	0.213
Kinematic	n^b	2.5
Hardening	h_0	7.93
	c_h	1.14
Fabric dilatancy	z_{max}	25
	c_z	1000

The experimental data of Gulf of Mexico clay used in this study is limited to fast cyclic loading tests with the frequency of the cyclic shearing in the range of 0.1–0.2 Hz. Fast cyclic shearing of clay leads to apparent increase of its stiffness and strength. The model is rate independent and therefore does not have a mechanism to account for such increase. Without that, the shear strength of the model may not be sufficient to sustain the intended shear stress amplitudes in the stress-controlled cyclic shearing simulations; hence the simulations may quickly lead to the critical state and infinite shear strains without even reaching the desired shear stress amplitudes. To prevent this problem, a virtual increase of the size of the bounding surface is adopted in all simulations in order to partially account for this shortcoming of the model. Through iterative procedure it is found that for these cyclic loading simulations the initial p_0 should be increased by at least by a factor of 1.5, and therefore this factor is adopted for all of the present cyclic loading simulations.

The bounding surface parameters, h_0 and a_d, are calibrated by fitting the model simulation to the stress-strain loops of the 1-D linear test GOM-5 (see Table 2). The corresponding simulation using the fitted values of bounding surface parameters is shown in Fig. 5 and compared with the corresponding experimental data. More details about the model calibration and simulation of the consolidation loading history are presented in Seidalinov [39].

4.2. Monterey No. 0/30 sand

The Monterey No. 0/30 sand database used in this study is from a testing program at the University of California, Berkeley [38,17]. To calibrate the model parameters of SANISAND, both monotonic and cyclic tests are required. The above reference database however only includes unidirectional and multidirectional cyclic shear tests. Although the Monterey No. 0/30 sand was also used as the standard laboratory testing sand at the University of Colorado, Boulder [40,41], it has been reported by Wu [38] that this type of Monterey No. 0/30 sand at the University of Colorado is substantially different from the sand at the University of California, Berkeley. In view of unavailability of monotonic tests on Monterey No. 0/30 sand, undrained monotonic triaxial tests on Monterey No. 0 sand from Riemer [42] are chosen for the calibration because both materials show the similarity in the respective gradation curves [38]. In this case, most of the parameters except fabric dilatancy parameters, z_{max} and c_z, which are pertinent to cyclic loading simulations, are calibrated based on Monterey No. 0 sand. For calibration of the fabric dilatancy parameters unidirectional cyclic shear tests from Wu [38] on Monterey No. 0/30 sand are used.

The detailed calibration procedure for SANISAND model parameters has been expounded by Taiebat et al. [36]. Based on the small strain domain of the deviatoric stress and axial strain curves provided in [42] from several monotonic triaxial compression tests, an initial estimate is made for the shear modulus coefficient G_0. Based on the critical state information from monotonic triaxial compression tests, the model parameters related to the critical state line (CSL) are found from curve fitting. Some other model parameter are typically found by a trial-and-error procedure for matching certain aspects of stress-strain response; e.g., ν, m, n^d, A_0, n^b, h_0 and c_h are found from monotonic loading, and z_{max} and c_z from cyclic loading. In the present study, given the considerable size of the experimental database, instead of using the inefficient trial-and-error procedure, an optimization algorithm by Liu et al. [43] is used for faster and better calibration of these model parameters. With the CSL parameters fixed and an initial guess on G_0, plus reasonable guesses on the initial value and bounds of the other model parameters except c_z and z_{max} related to cyclic test, three undrained triaxial compression tests are chosen to build the objective function. The optimization result is shown in Fig. 6. Later, c_z and z_{max} are determined by trial and error procedure on dozens of cyclic DSS tests from [38]. An example of the results of the calibration procedure on cyclic DSS test is presented in Fig. 7. This set of results belong to a specimen consolidated under CK_0 to $\sigma'_{vc} = 85$ kPa with a relative density $D_r = 75\%$ and then subjected to undrained DSS with CSR = 0.447. The complete list of the calibrated parameters is given in Table 5.

For the above mentioned cyclic loading scenarios on Monterey sand and the subsequent multidirectional simulations presented in the next section, the initial conditions considered for the numerical simulations are that of the end of the consolidation stage from the experiments. In other words, the initial consolidation stage is not simulated by SANISAND. This is partly because it is usually difficult to obtain the sample information such as the void ratio prior to the initial consolidation stage. In addition this version of SANISAND does not consider effects from the initial fabric, so there is not much point in trying to simulate the sample state during the consolidation stage. As the lateral normal stresses are not measured in the experiments, to account for the initial CK_0 and CK_α conditions an assumption is made that both initial lateral normal stresses are equal to half of the initial effective vertical stress σ'_{vc}, i.e., $K_0 = 0.5$ for both types of samples.

5. Simulation results for multidirectional cyclic loading

Based on the parameters calibrated in the previous section, the SANICLAY and SANISAND models are used here for illustration of their simulative capabilities; each one in simulation of ten related multidirectional cyclic shear tests. The simulated cyclic shear paths include 1-D and 2-D linear, circular/oval, and figure-8 type A. From the large number of tests that are simulated, detailed results are presented for only selected ones. Then selected aspects are the results for all of the tests are summarized at the end.

Some of the presented results are in terms of shear stress magnitude $\tau = \sqrt{\tau_x^2 + \tau_y^2}$ and shear strain magnitude $\gamma = \sqrt{\gamma_x^2 + \gamma_y^2}$. Of course in the 1-D linear path, these yield to $\tau = \tau_x$ and $\gamma = \gamma_x$ due to the absence of the τ_y and γ_y components. In the presentation of the selected complete sets of the results two layouts are considered, each consisting of four subplots.

(i) For 1-D and 2-D linear paths, normalized stress path (τ/σ'_{vc} against σ'_v/σ'_{vc}), and stress-strain path (τ/σ'_{vc} against γ) are plotted as the top two subplots of the layout. Accumulation of pore pressure ratio with number of cycles ($\Delta u/\sigma'_{vc}$ against N) and accumulation of shear strain magnitude with number of cycles (γ against N) are plotted as the bottom two subplots of the layout.

(ii) For circular/oval and figure-8 type A paths, normalized shear stress path (τ_y/σ'_{vc} against τ_x/σ'_{vc}), and shear strain path (γ_y against γ_x) are plotted as the top two subplots of the layout. The bottom two subplots of this layout are same as those used for 1-D and 2-D linear paths.

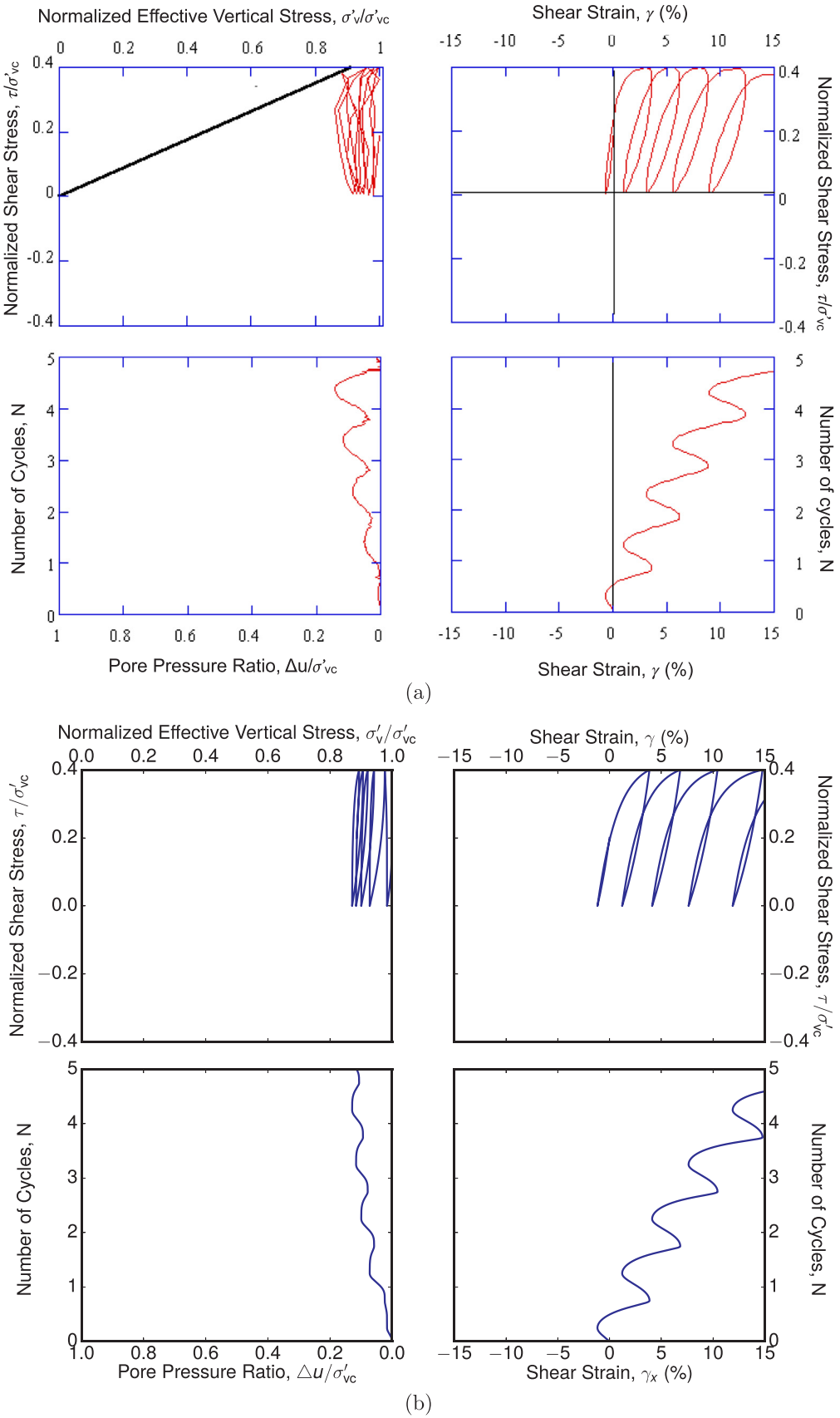

Fig. 8. Simulation versus experiment in 1-D linear multidirectional cyclic shear test GOM-6 on Gulf of Mexico clay: (a) experiment [18] and (b) simulation.

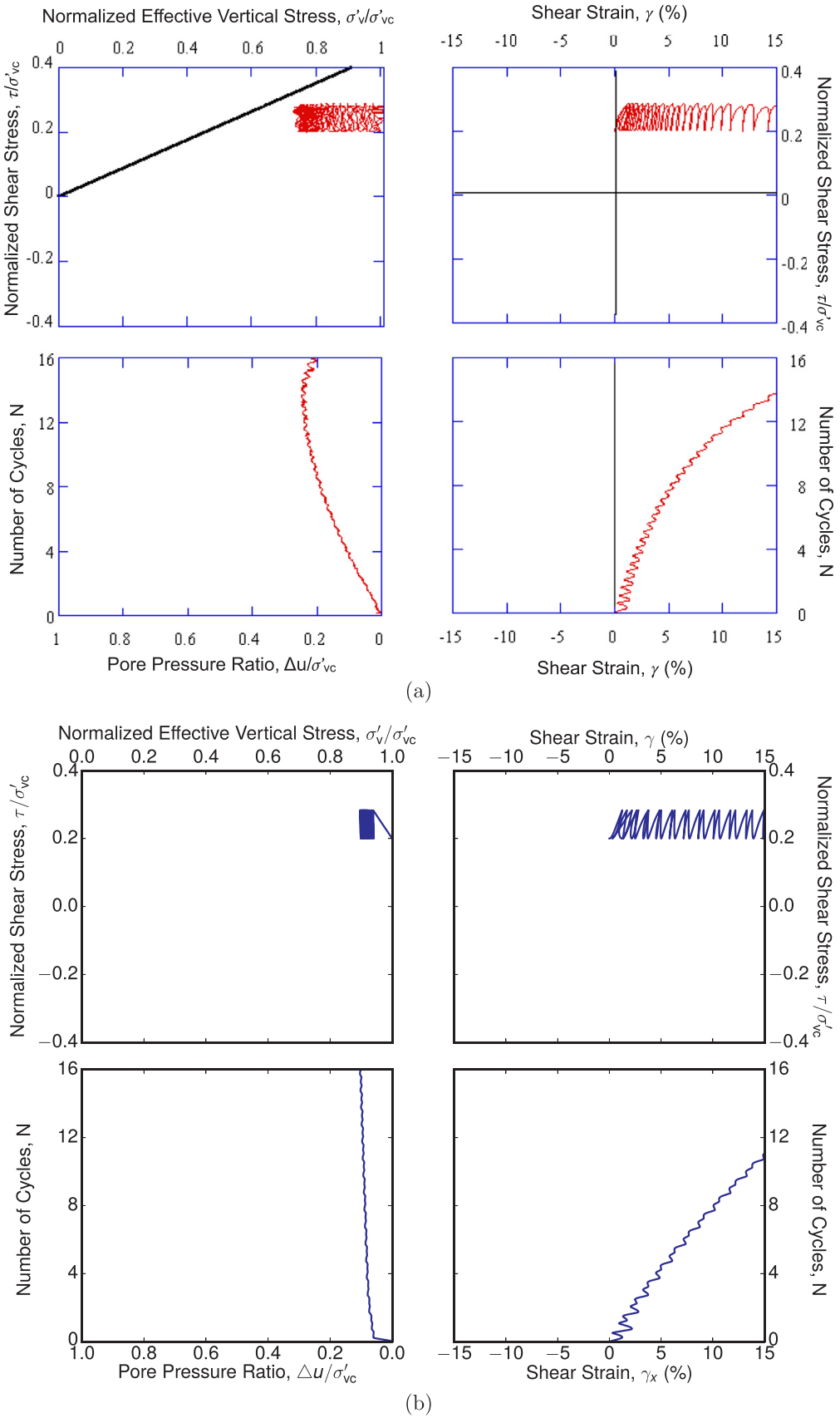

Fig. 9. Simulation versus experiment in 2-D linear multidirectional cyclic shear test GOM-8 on Gulf of Mexico clay: (a) experiment [18] and (b) simulation.

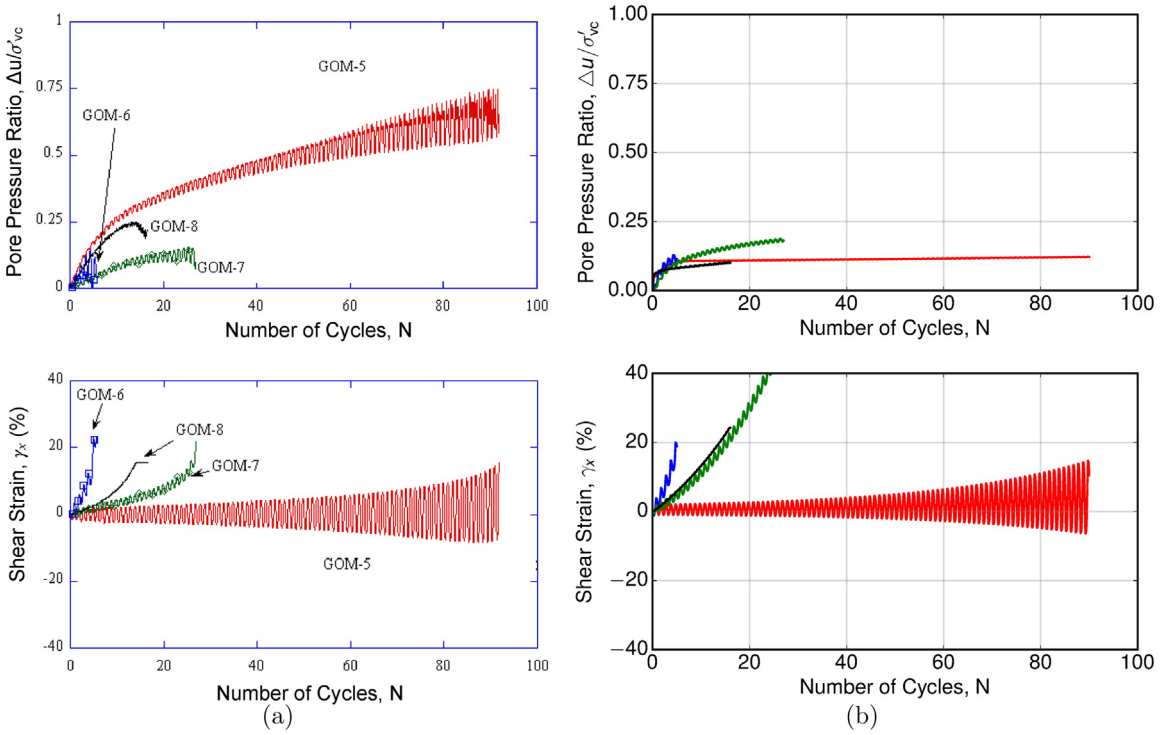

Fig. 10. Simulations versus experiments in 1-D and 2-D linear multidirectional cyclic shear tests on Gulf of Mexico clay: (a) experiment [18] and (b) simulations.

The layout of the summary plots consists of accumulation of pore pressure ratio with number of cycles ($\Delta u/\sigma'_{vc}$ vs. N), and accumulation of shear strains with number of cycles (γ_x and γ_y vs. N). Due to unavailability of the digitized data for Gulf of Mexico clay, summary plots for simulation results for 1-D and 2-D linear paths are plotted together in accordance with the corresponding experimental plots as presented in the related reference.

5.1. Gulf of Mexico clay

For the Gulf of Mexico clay, ten sets of test results are considered for evaluation of the SANICLAY model performance. These include three 1-D linear, one 2-D linear, three circular, and three figure-8 type A shear paths.

5.1.1. 1-D and 2-D linear stress paths

Aside from the 1-D linear path GOM-5 without initial shear stress that was used for calibration of h_0 and a_d parameters in Section 4.1, a complete set of simulation results for 1-D linear path GOM-6 with $SSR_x = 0.2$ is shown in Fig. 8. The accumulation of the pore pressure in the simulation follows a similar trend as that in the experiment with increasingly larger amplitudes as the number of cycles increases for the experiment. Shear strain γ also follows a very similar trend in the simulation and the experiment. The amplitude of shear strain γ is simulated close to the experiment as the number of cycles increases.

A complete set of simulation results for 2-D linear path GOM-8 with $SSR_x = 0.2$ is shown in Fig. 9. The pore pressure ratio in the simulation develops much faster than that in the experiment at the very beginning of the cyclic loading, followed by a smaller accumulation trend afterwards. In the experiment, however, the accumulation of pore pressure is gradual and continues up to about the 14^{th} cycle, after which the pore pressure starts reducing. At the end of the 16^{th} cycle, the model simulates pore pressures that are about half of those in the experiment. The trend followed by the shear strain accumulation in the simulation is similar to that in the experiment with a minor difference in the rate of accumulation.

Comparison between the results of simulations and experiments for all of 1-D and 2-D linear stress paths are summarized in Fig. 10, including results of GOM-5, GOM-6, GOM-7, and GOM-8. While the simulations of pore pressure ratio are poor, accumulation of the shear strain γ_x with the number of cycles is simulated relatively well for all of the tests. Note that test data of GOM-5 is the one used for calibration of the bounding surface model parameters.

5.1.2. Circular stress path

A complete set of simulation results for circular test GOM-11 with $SSR_x = 0.2$ is presented in Fig. 11. The accumulation of the pore pressure ratio is positive in the experiment but negative in the simulations, with values that are outside the plotting limits; these are plotted separately in Fig. 12 for all of the simulated circular stress paths. Shear strains simulated by the model are following a slightly different trend with well captured accumulation of the shear strain γ_x and overestimation of accumulation of the shear strain γ_y.

The results of the simulations and experiments for all circular multidirectional cases are summarized in Fig. 13, including results of GOM-10, GOM-11, and GOM-12. The model simulations of pore pressure ratios are not in agreement with the experiments. For GOM-10 with $SSR_x = 0$ the problem is about the magnitude of pore pressure, but for the other two cases with $SSR_x = 0.2$ it is also about the negative (although small) rate of pore pressure simulated in the first few cycles. In terms of the accumulation of shear strains in both directions, the simulations for the GOM-11 and GOM-12 with $SSR_x = 0.2$ appear to be very good, with more success for simulation of accumulation of shear strain along the x direction that is the direction of the initial offset shear stress. For these two cases, as expected the accumulation of shear strains in the other direction is significantly smaller. For the GOM-10 with $SSR_x = 0$, the shear strains in the experiments show higher and increasing magnitude while the simulated ones appear to show smaller

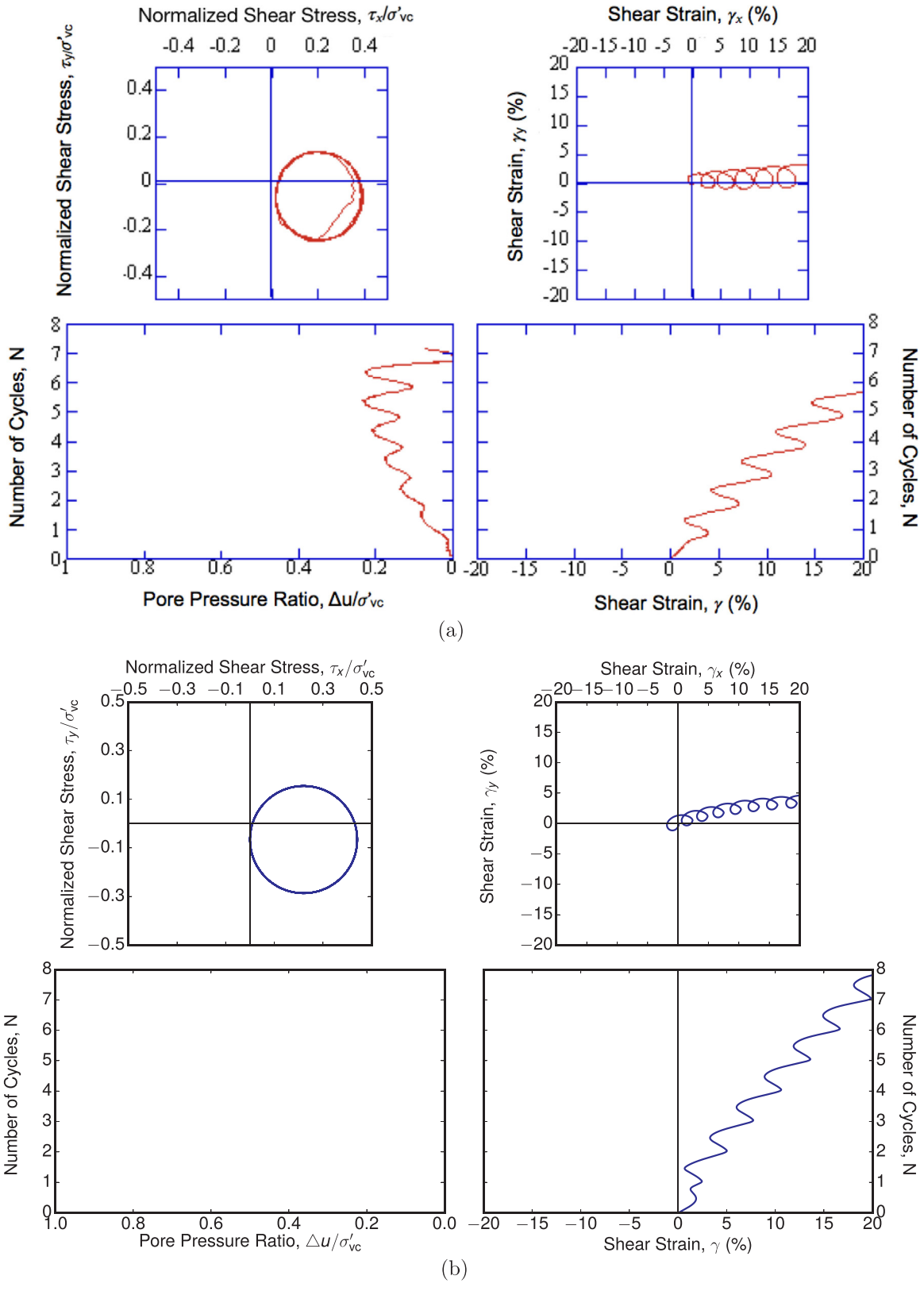

Fig. 11. Simulation versus experiment in circular/oval multidirectional cyclic shear test GOM-11 on Gulf of Mexico clay: (a) experiment [18] and (b) simulation.

and nearly constant magnitude.

5.1.3. *Figure-8 type A stress path*

A complete set of simulation results for figure-8 type A test GOM-14 with $SSR_x = 0.2$ is shown in Fig. 14. The experimental results and the model simulations are presented for only about three cycles of loading. Despite the very complex nature of this loading path, the model simulations are in very good agreement with the experimental results. The pore pressure variation follows the same trend in the simulation as in the experiment, with slightly smaller amplitude in the third cycle of

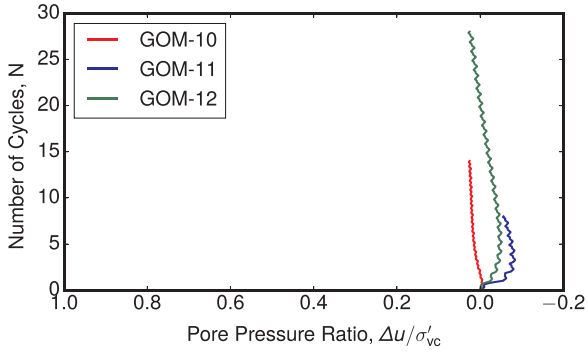

Fig. 12. Initially negative accumulation of simulated pore pressure for circular multidirectional cyclic shear tests: GOM-10, GOM-11 and GOM-12.

the simulation. The experimental results of the shear strains show variation around $\gamma_y = 0$ and accumulations along the γ_x axis. The simulation captures the trend but shows slight deviation from the experiment with the accumulation of the shear strains in the negative γ_y direction. The magnitude of shear strain is captured well with the number of cycles.

The results of the simulations and experiments for all figure-8 type A multidirectional tests are summarized in Fig. 15. Here, in contrast to the circular stress path, the model simulates positive pore pressure ratios as observed in the experiments but only at a smaller rate. In terms of the accumulation of the shear strains, simulation of figure-8 test GOM-13 with $SSR_x = 0$ suggests smaller amplitudes compared to those of the experiments, with proper residual trend for the γ_x and not the γ_y. The simulation results for GOM-14 and GOM-15 with $SSR_x = 0.2$ are comparable qualitatively and quantitatively well with the experimental results in terms of the accumulation of γ_x. This is also the case for simulations of the accumulation of γ_y, with more success for GOM-14 with larger CSR values compared to GOM-15.

5.2. Monterey No. 0/30 sand

Simulations against experiment results for Monterey No. 0/30 are provided next. The tests include two 1-D linear, two 2-D linear, three circular/oval, and three figure-8 type A shear paths.

5.2.1. 1-D and 2-D linear stress paths

A complete set of simulation results for one 1-D linear path test ms67cyck with initial static shear stress is presented in Fig. 16. The model captures the contractive and dilative parts of various cycles, and with a slightly faster pace than the experiment it reaches the non-symmetric "butterfly" stress orbit where it better captures the cycles of excess pore pressure variation. In terms of shear strains development,

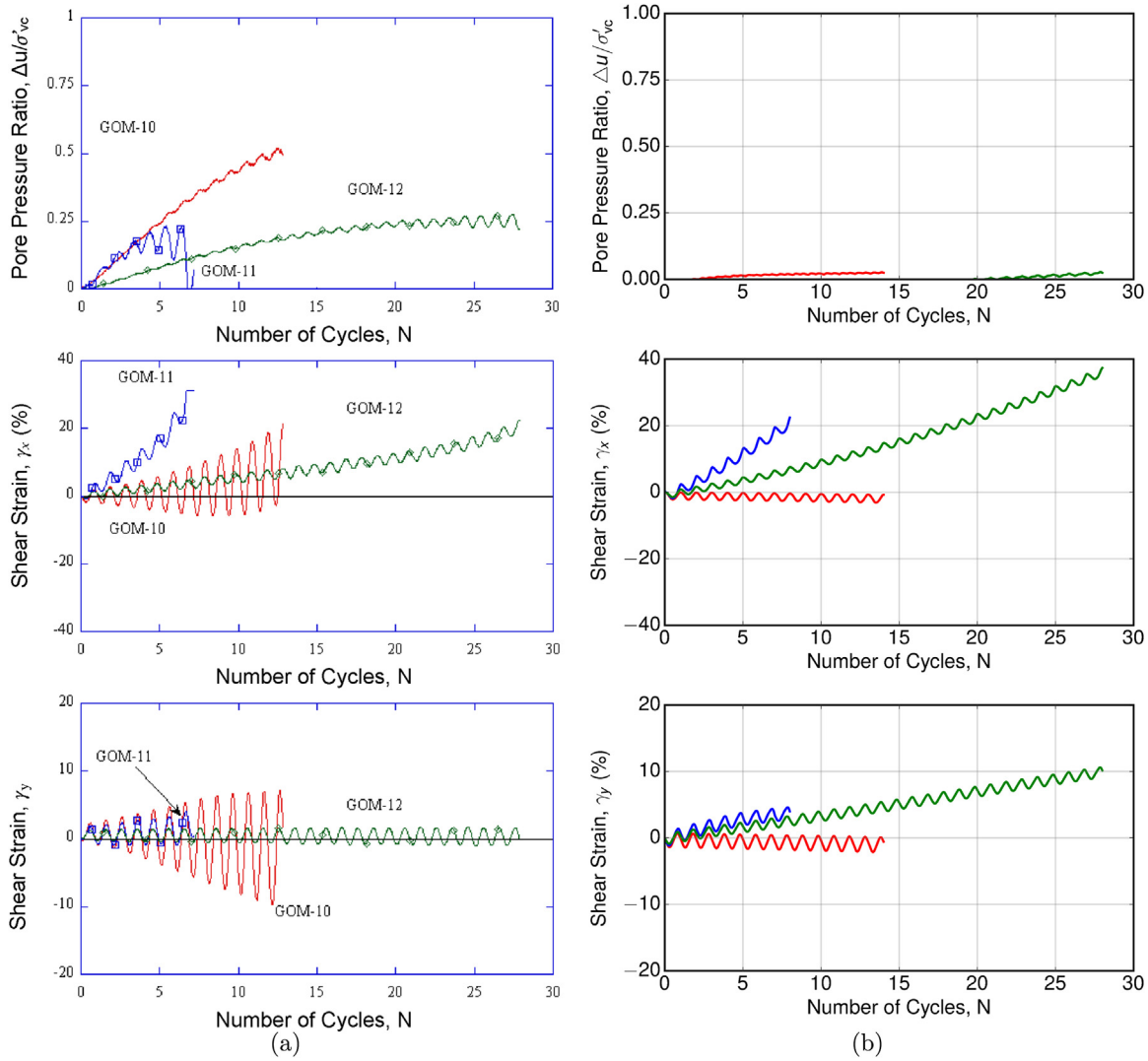

Fig. 13. Simulations versus experiments in circular/oval multidirectional cyclic shear tests on Gulf of Mexico clay: (a) experiments [18] and (b) simulations.

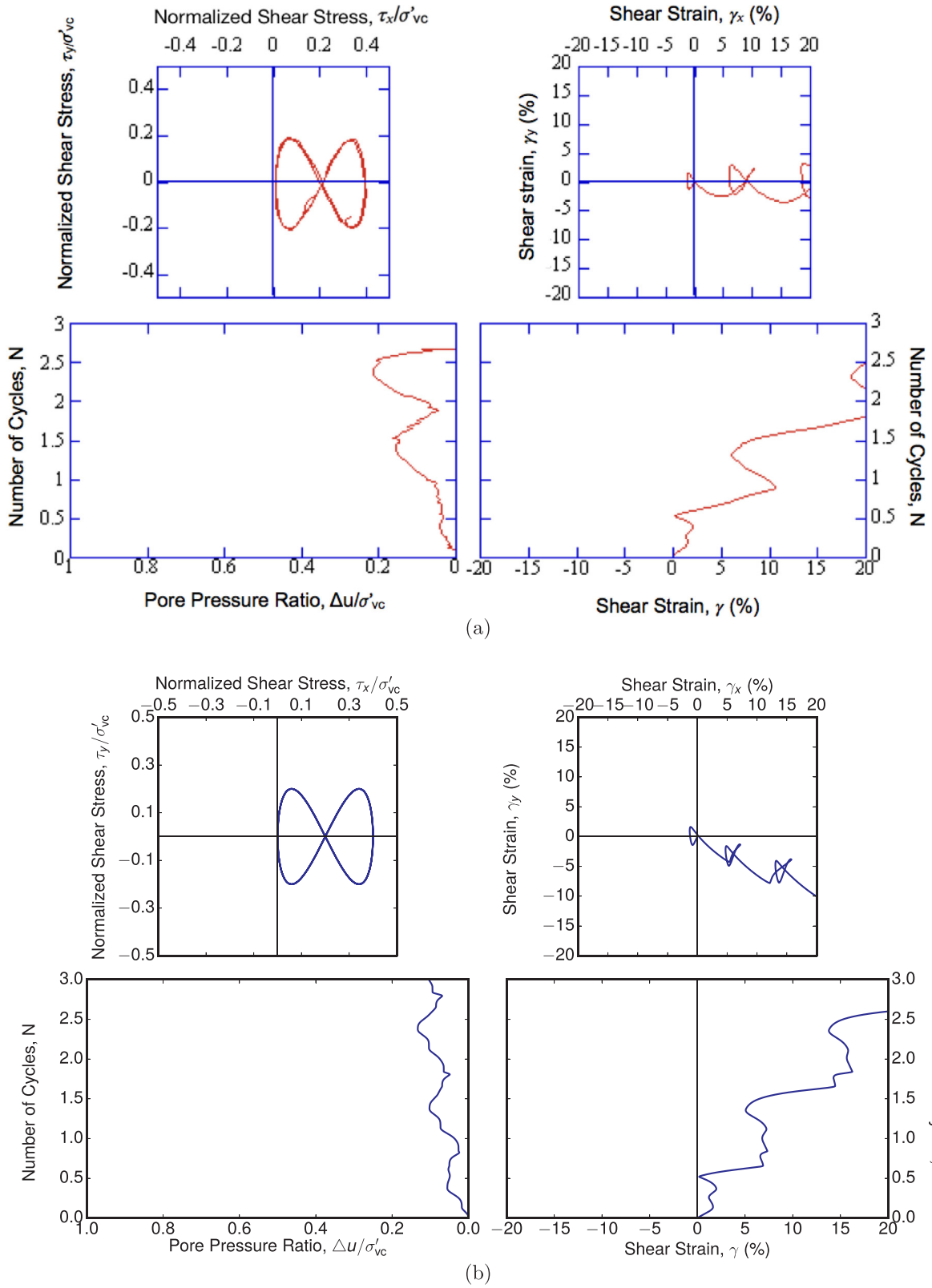

Fig. 14. Simulation versus experiment in figure-8 type A multidirectional cyclic shear test GOM-14 on Gulf of Mexico clay: (a) experiment [18] and (b) simulation.

the simulated stress-strain curve tends to shift along the initial static shear stress direction with smaller amplitudes of oscillation than those in the experiment. It appears that in the reverse loading cycles toward decreasing of shear stress, the model does not generate as much reversal strain as those observed in the experiment, and this is why the strain path tends toward the positive shear strain direction.

Comparison between experiments and simulation results for the two selected 1-D linear tests is summarized in Fig. 17, including results of

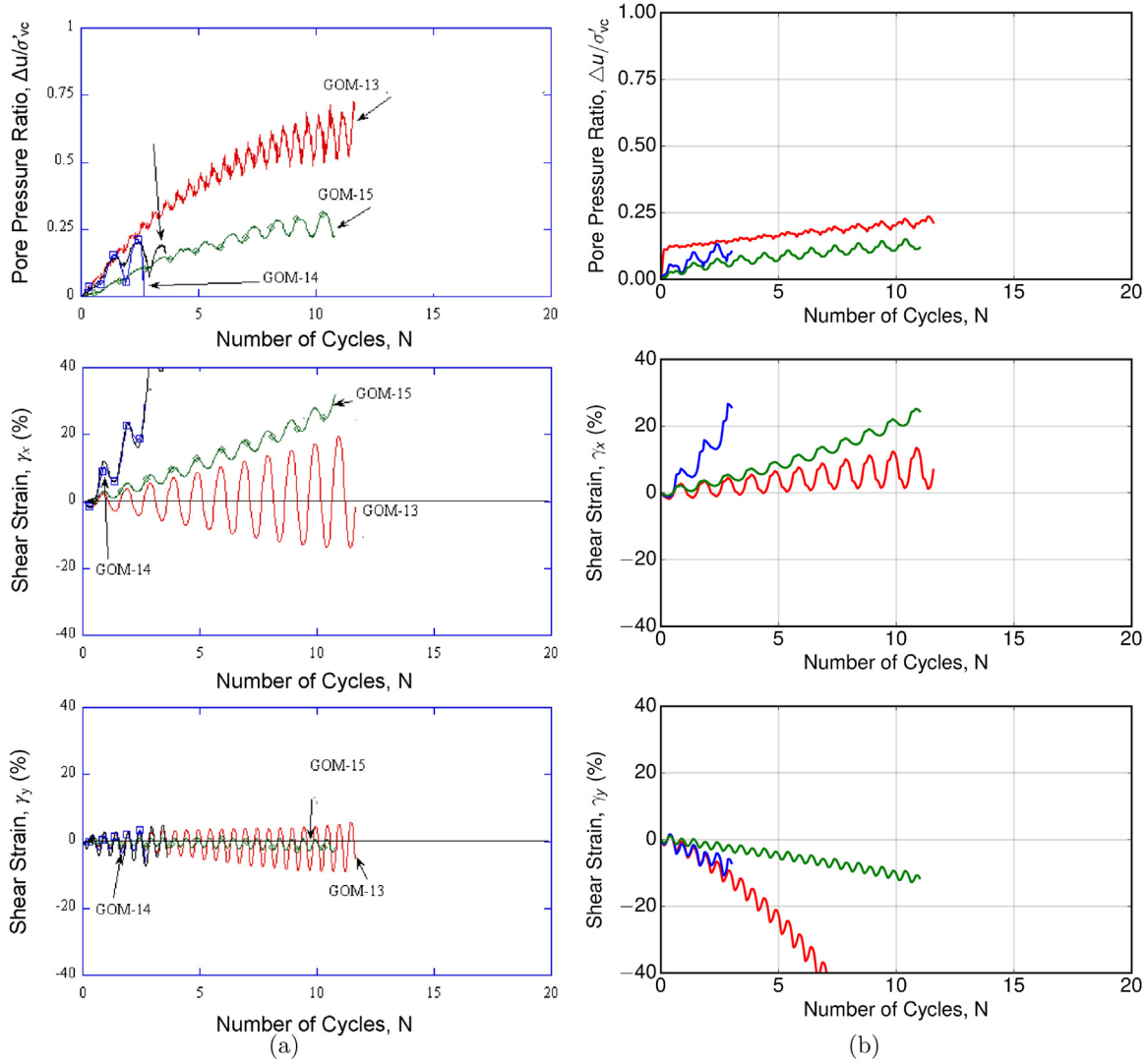

Fig. 15. Simulations versus experiments in figure-8 type A multidirectional cyclic shear tests on Gulf of Mexico clay: (a) experiments [18] and (b) simulations. Note: experimental data of figure-8 type B (black line in the experiment results) is not included in simulation results.

ms66cyck and ms67cyck. Simulations of pore water pressure are in acceptable agreement with the experiments in terms of both accumulation and oscillation, while simulations of shear strain γ_x overestimate the observed pace of accumulation from the experiments for the two CSRs.

A complete set of simulation results for a 2-D linear test ms61cyck is shown in Fig. 18. The model is successful in simulating the trend of pore pressure accumulations, although again a bit faster than the experiments in the beginning of the cyclic loading. Given the shear stress path shown in this figure, the simulated shear strain orbit reveals that the model behaves softer than the experiment along the initial static shear stress direction. Note that, with x and y referring to the intended slope dip and strike directions, respectively, this type of loading can be seen as a problem that an element of soil under a slope (hence under initial shearing in the slope dip direction) is subjected to an unidirectional earthquake along the slope strike direction. Similar to the experiment, the simulation indicates that accumulation of considerable shear strain should be expected along the slope dip direction, and it is insightful that the model captures this phenomenon.

Comparison between experiments and simulation results for 2-D linear tests is summarized in Fig. 19, including results of ms60cyck and ms61cyck. Simulations of pore pressure are in good agreement with the experiments in terms of the accumulation, but with slightly smaller oscillation magnitudes in each cycle. For the shear strain along the initial static shear stress direction γ_x, the average trend of the simulations is good but the model behaves softer than the experiment. In particular, after the first few cycles, the model seems to exhibit a nearly constant shear stiffness for all subsequent cycles, while in the experiment the stiffness appears to have an increasing trend with the number of cycles. From those two experiments, it is easy to assert that the mobilized maximum pore pressure ratio does not reach beyond 0.8 but the accumulated shear strain can go beyond 10%. This contradicts a very common assumption that large deformation is usually induced by liquefaction with pore pressure ratio of around 1.0.

5.2.2. *Circular/oval stress path*

A complete set of simulation results for a circular/oval test ms35cyck with a medium SSR_x is presented in Fig. 20. The model still performs very well in capturing pore pressure accumulation, with a slightly faster pace of reaching to the nearly locked orbits in each cycle.

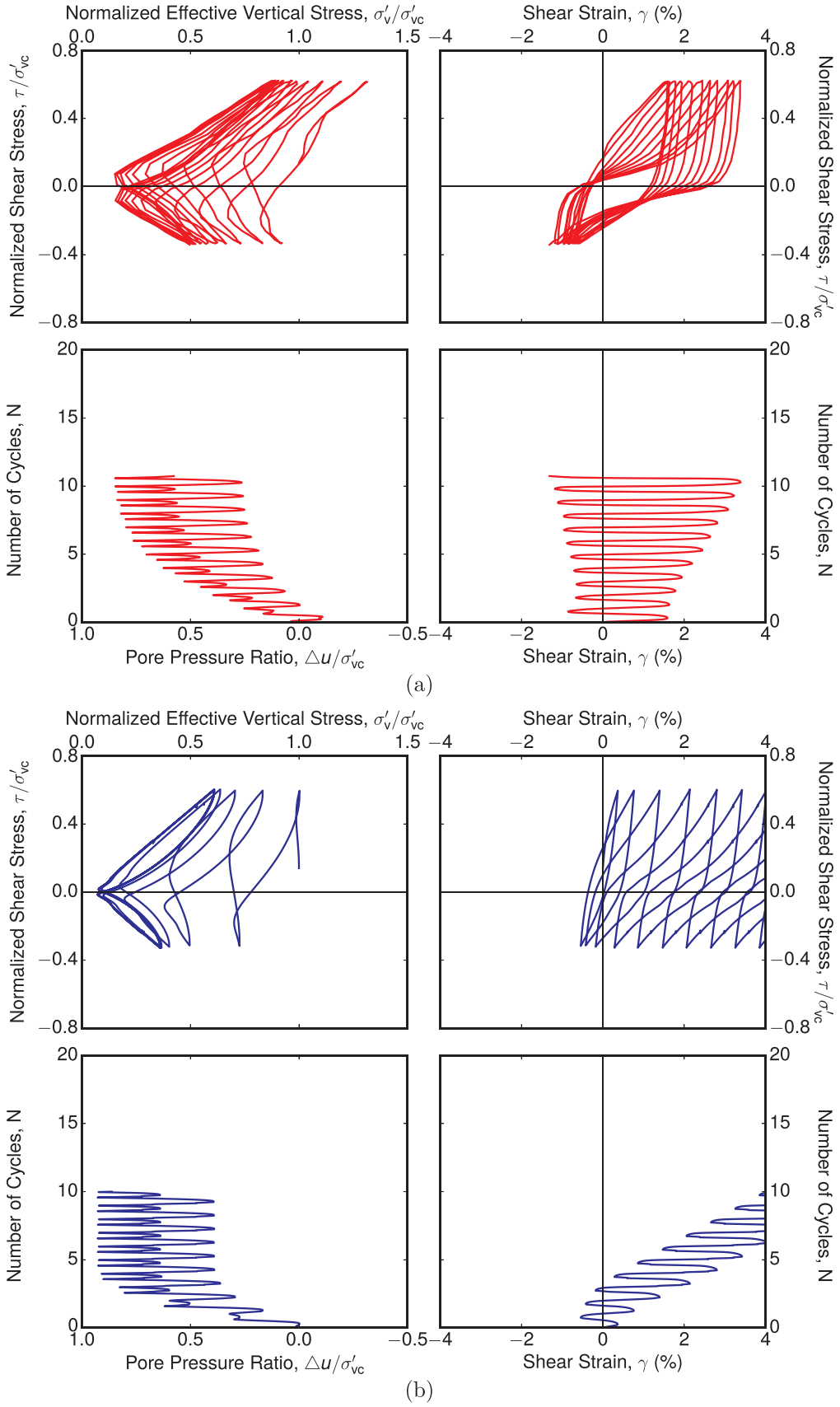

Fig. 16. Simulations versus experiments in 1-D linear multidirectional cyclic shear test ms67cyck on Monterey No. 0/30 sand: (a) experiment [17] and (b) simulation.

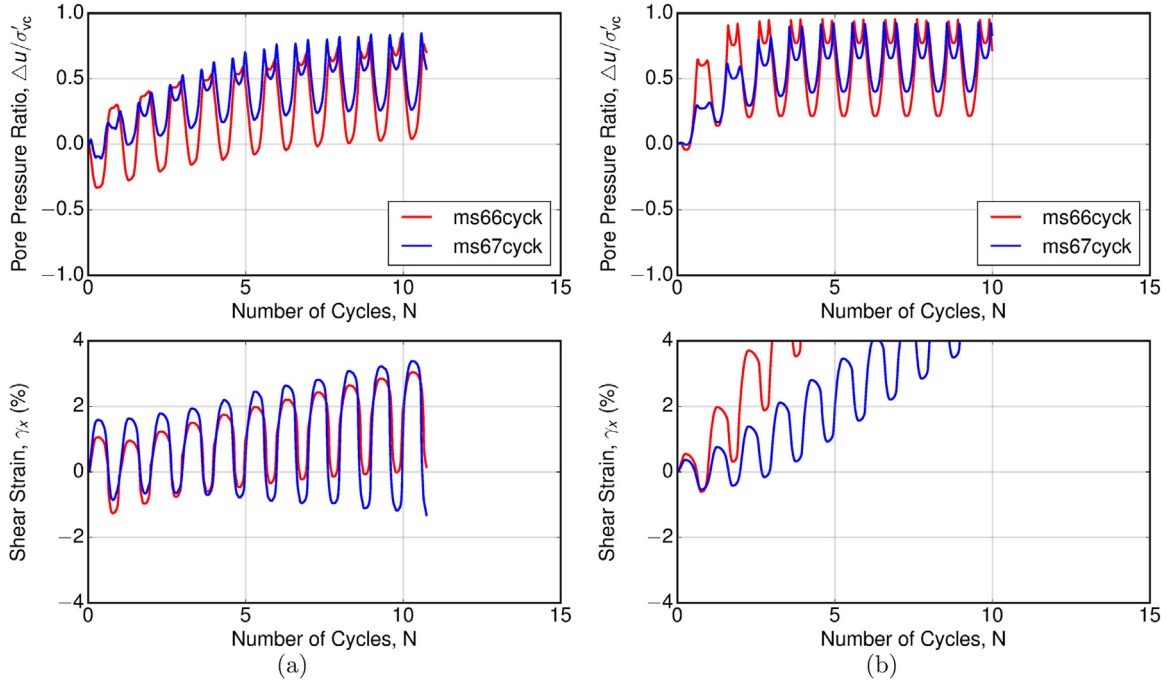

Fig. 17. Simulations vs experiments in 1-D linear multidirectional cyclic shear tests on Monterey No. 0/30 sand: (a) experiments [17] and (b) simulations.

The simulated strain orbit seems to deviate noticeably from the experiment. One can argue that this may share the same reason with the 1-D linear case in Fig. 16 where the shear strain is not able to expand on both sides. Nevertheless, careful examination of the resultant strain shows that the model captures well the average strain in each cycle, and the main problem there is missing the magnitude of the oscillations in each loading cycle.

Experiments and simulation results for circular/oval multidirectional cyclic shear tests are summarized in Fig. 21, including results of ms44cyck, ms35cyck, and ms59cyck. Model simulations of accumulation of pore pressure are quite similar to those observed in the experiments, with slight under-prediction of the magnitude of the oscillations. As for two shear strains of γ_x and γ_y, the model exhibits very good qualitative simulations on the development trend, but missing the amplitude of the cycles as observed and discussed before. Roughly speaking, for the element test without or with initial static shear bias, i.e., ms44cyck, the simulated strain path tends to stay around zero while the experiment produces shear strains oscillating around 0% and increasing in magnitude up to about 10% for both γ_x and γ_y with the number of cycles. For the element test with a medium SSR_x, i.e., ms35cyck, shear strains can develop and accumulate to larger values.

5.2.3. Figure-8 type A stress path

A complete set of simulation results for a figure-8 type A test ms38cyck with a medium SSR_x is presented in Fig. 22. The results of the model simulation with respect to the reported experiments, in terms of both pore pressure and shear strains show similar trends as those observed in the oval stress path of Fig. 20. Again here, the trend of the average response in terms of both pore pressure and resultant shear strain appears to be successful, however the oscillation magnitudes in each cycle are not captured properly.

Experiments and simulation results for figure-8 type A multidirectional cyclic shear test are summarized in Fig. 23, including results of ms33cyck, ms38cyck, and ms52cyck. The whole picture tells a similar story to circular/oval path in Fig. 21. The model performs very well in simulating the average trend of the pore pressure generations, and it under-predicts the magnitude of oscillations in each cycle of loading. As for shear strain accumulation, the general trend is picked up by all the three simulations, although for relatively small SSR_x cases, i.e., ms33cyck and ms38cyck, simulations could not produce the oscillations with large magnitude.

5.3. Summary

Selected versions of SANICLAY and SANISAND bounding surface plasticity models were evaluated in modeling multidirectional cyclic shear tests on Gulf of Mexico clay and Monterey No. 0/30 sand, respectively. The shearing paths examined include 1-D and 2-D linear, circular/oval and figure-8 type A. The total of twenty experiments examined reveal a lot of information about the complexity of the material response and the capabilities and limitations of the two models. A summarized comparison of the simulated and measured response for these twenty tests are presented in Fig. 24. For each case, the comparison is made at the end of a selected cycle number as shown in the legend of this figure. While the selected cycle numbers vary for the clay tests (for which the digitized data of experiments was not available to the authors), they are consistently selected as 10 for the sand experiments. The results at the end of selected cycles are compared in terms of pore pressure ratio and shear strains γ_x and γ_y. The horizontal and vertical axes of each plot represent values from the experiments and simulations, respectively, with the diagonal dashed line representing the ideal situation of perfect match between the experimental and simulation results. This method of comparing the experiments as simulations at the end of selected loading cycles does not reveal many detailed aspects of the cyclic response; yet it is a way of getting an overall comparison in dealing with this extensive amount of information.

Performance of the SANICLAY model is summarized in Fig. 24(a). Based on what is presented in this figure, and the detailed results

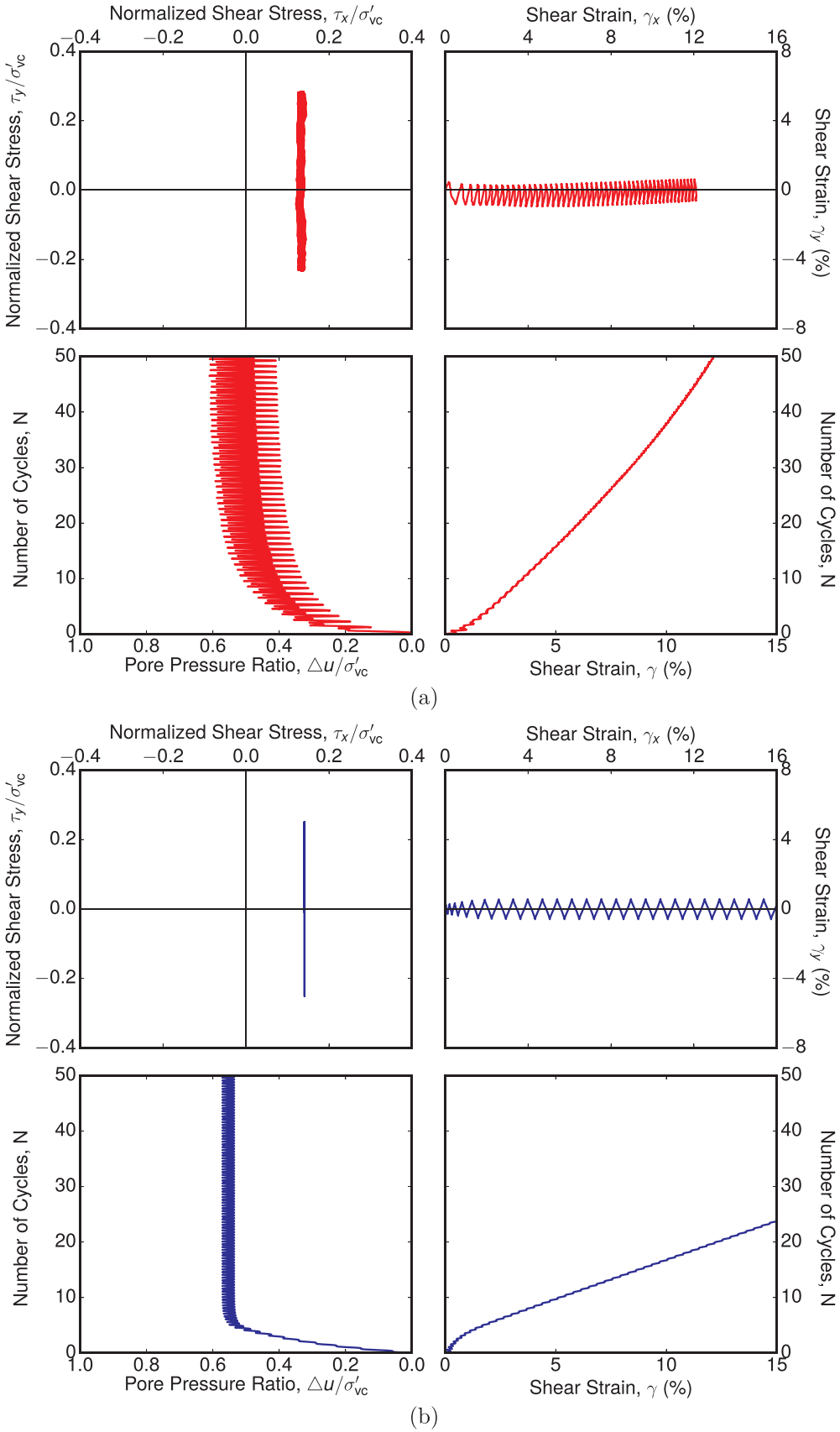

Fig. 18. Simulation versus experiments in 2-D linear multidirectional cyclic shear test ms61cyck on Monterey No. 0/30 sand: (a) experiment [17] and (b) simulation.

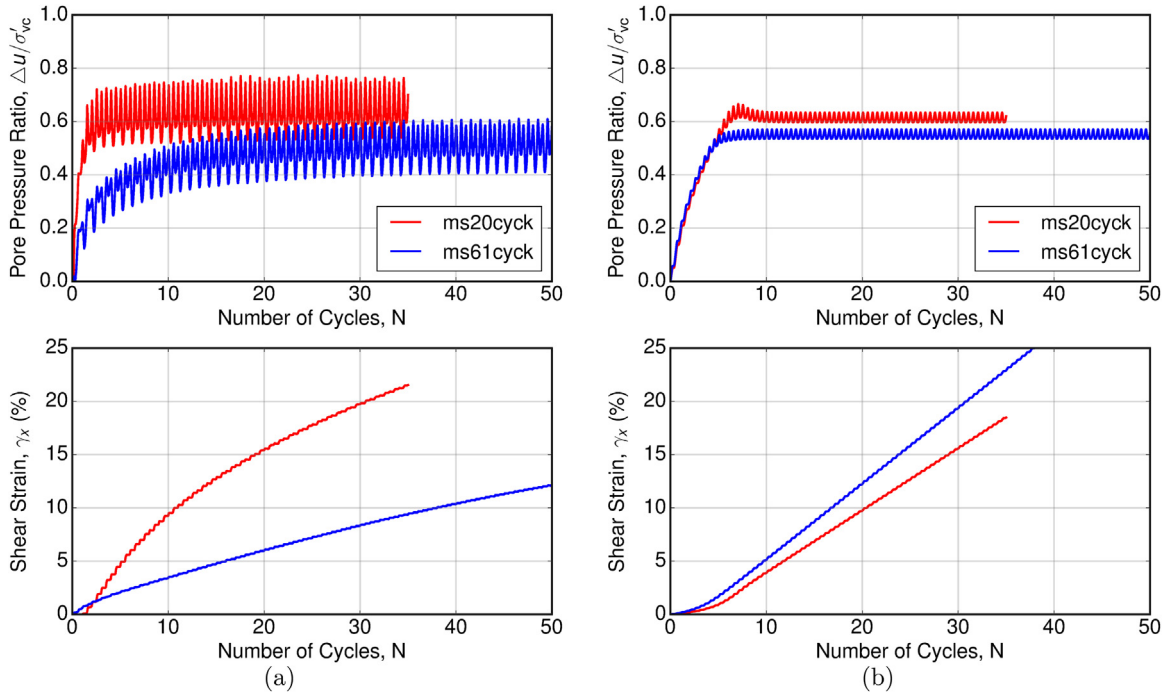

Fig. 19. Simulations versus experiments in 2-D linear multidirectional cyclic shear tests on Monterey No. 0/30 sand: (a) experiments [17] and (b) simulations.

presented in the previous figures, the observations can be summarized as follows. In many of the simulation results, particularly those with $SSR_x = 0$ the accumulation of pore pressure ratio is significantly under-predicted. This could be attributed to the increased size of the bounding surface prior to cyclic loadings, in order to indirectly account for the rate effect from the fast cyclic loading used in the experiments, as discussed under the calibration of the clay model. Model performance in terms of accumulated shear strains is perceived as satisfactory with enough room for further refinements of its simulative capabilities, in particular for specimens with $SSR_x = 0$ values. Accumulated γ_x values are somewhat under-predicted with the most deviations observed for circular and figure-8 type A loadings on specimens with $SSR_x = 0$. Accumulated γ_y values are in acceptable range, again except for figure-8 type A loading on specimens with $SSR_x = 0$.

Performance of the SANISAND model is summarized in Fig. 24(b) with the sampling points selected at cycle 10. The model simulates pore pressure ratio in good agreement with the experiments except for the circular/oval test ms59cyck, and figure-8 type A test ms52cyck, both with large SSR_x. The accumulated γ_x values are well simulated except for the 1-D linear test ms66cyck where the model response is too soft, and figure-8 type A test ms52cyck where the model could not capture oscillations with large magnitude. The accumulated γ_y values are scattered along 1:1 line but show the good trend. Note that almost all the related points are located in the first and third quarters of the plot, which means that simulation results share the same sign with the experiments.

6. Evaluating the proximity to neutral loading

In an attempt of revealing potential shortcoming in the models, an investigation is conducted next on the proximity of the applied stresses to the neutral loading. Taiebat and Dafalias [44] recently pointed out the stress reversal surface models and the generalized plasticity models are not truly zero elastic range models, even when they are intended to be, and they produce pure elastic response for the so called neutral loading path that are normal to the "loading direction". It should be emphasized that in reality soils are not expected to exhibit purely elastic response, and the neutral loading is merely an artificial response of many constitutive models. The SANICLAY and SANISAND models inherit the possibility of facing neutral loading condition as they fall in the category of models with stress reversal surfaces. It is therefore interesting to examine these models in the complex stress paths explored in this study.

For the bounding surface formulation of SANICLAY, the neutral loading would occur when the loading path $\dot{\boldsymbol{\sigma}}$ is tangential to the loading surface $f = 0$, that is the surface passing through current stress state $\boldsymbol{\sigma}$ and homologous to the bounding surface with the center of homology represented by the projection center $\boldsymbol{\sigma}_c$. In other words, the neutral loading for SANICLAY takes place when $(\partial f/\partial \boldsymbol{\sigma})$: $\dot{\boldsymbol{\sigma}} = 0$ with $\partial f/\partial \boldsymbol{\sigma}$ being a gradient of the loading surface in the generalized multiaxial stress space, $\dot{\boldsymbol{\sigma}}$ being the stress increment in the stress controlled simulations, and : representing the inner product operator. For SANISAND, the neutral loading would occur when the loading path $\dot{\mathbf{r}}$ is tangential to the yield surface in the stress ratio space. In other words, the neural loading for SANISAND takes place when $\mathbf{n}$: $\dot{\mathbf{r}} = 0$ with $\mathbf{n}$ being a gradient of the yield surface in the stress ratio space and $\dot{\mathbf{r}}$ being the stress ratio increment in the stress controlled simulations.

In a complex loading path, one can quantify the proximity of the model response to neutral loading by continuously examining the angle Θ between the loading direction and the stress increment. When $\Theta = 90°$, the neutral loading takes place and the model produces a purely elastic response. For the multidirectional cyclic shear paths, the variation of Θ is expected to be significant. For SANICLAY, Θ is the angle between $\partial f/\partial \boldsymbol{\sigma}$ and $\dot{\boldsymbol{\sigma}}$. For SANISAND, Θ is the angle between $\mathbf{n}$ and $\dot{\mathbf{r}}$. More specifically, for SANICLAY $\Theta = \arccos\left[((\partial f/\partial \boldsymbol{\sigma})\text{:}\,\dot{\boldsymbol{\sigma}})/(\|\partial f/\partial \boldsymbol{\sigma}\|\|\dot{\boldsymbol{\sigma}}\|)\right]$ where $\|\mathbf{x}\|$ represents the magnitude of tensor $\mathbf{x}$. In the formulation of SANICLAY with zero elastic nucleus, whenever $\Theta > 90°$, the stress reversal takes place and the

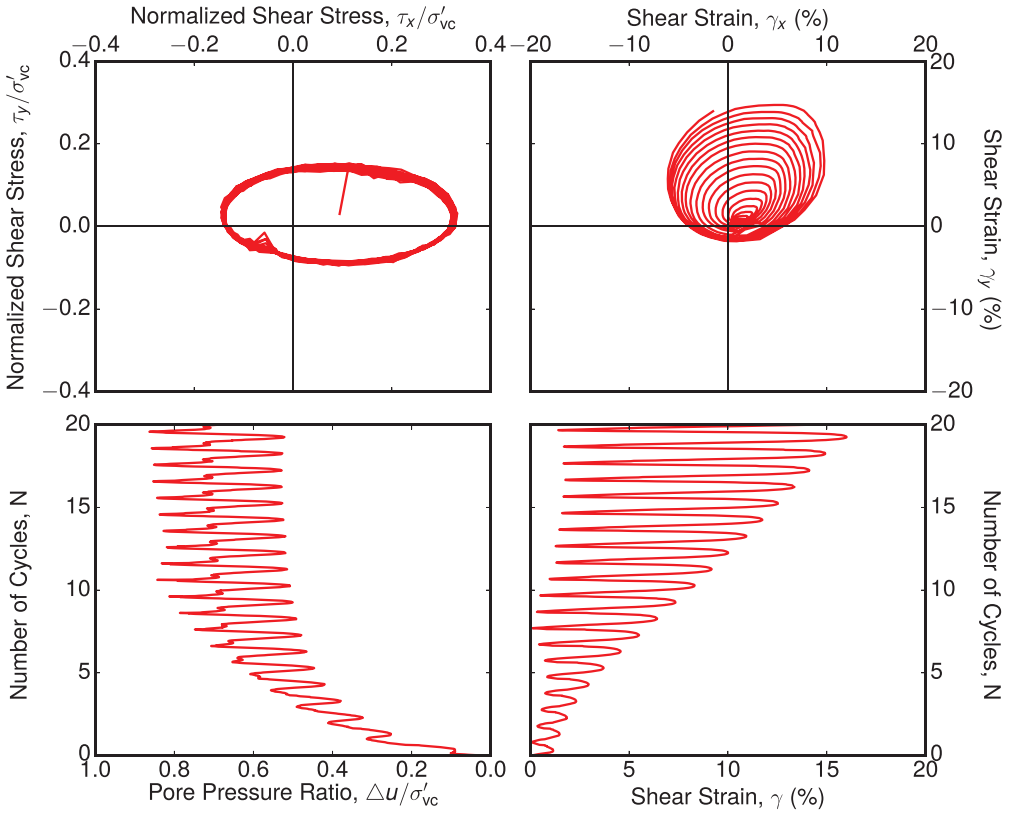

Fig. 20. Simulation versus experiment in circular/oval multidirectional cyclic shear test ms35cyck on Monterey No. 0/30 sand: (a) experiment [17] and (b) simulation.

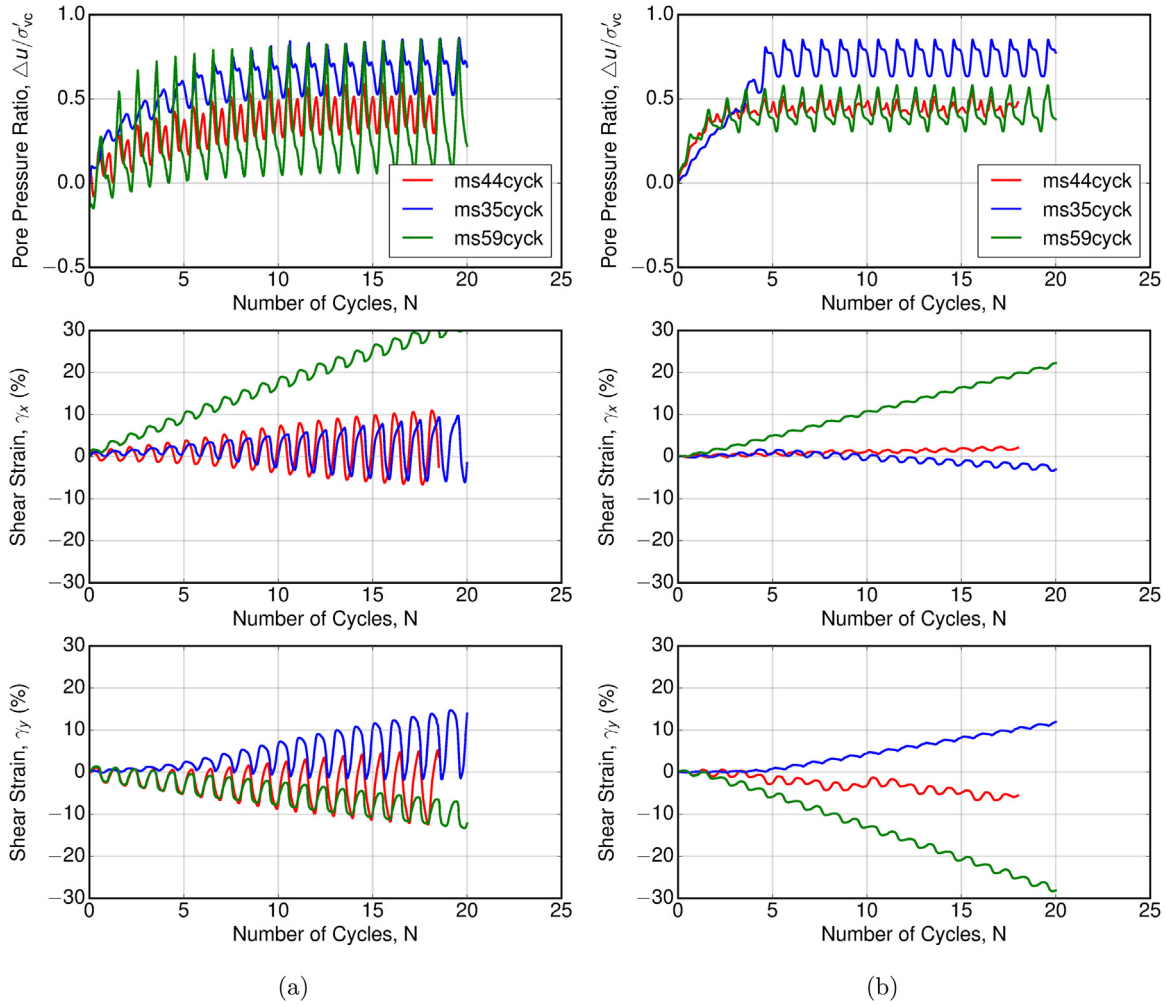

Fig. 21. Simulations versus experiments in circular/oval multidirectional cyclic shear tests on Monterey No. 0/30 sand: (a) experiments [17] and (b) simulations.

projection center is updated to that of current stress, thereby reducing the angle Θ. In this way, $\Theta \leq 90°$ is expected to be the case in all of the simulations of SANICLAY. The variations of Θ for selected 1-D linear, circular, and the figure-8 type A paths are plotted in Fig. 25 for the first 7 cycles of loading. For 1-D linear path, $\Theta \approx 20°$, suggesting that the loading scenario is not close to the neutral loading condition. For circular paths, Θ varies between 45° and 90° for GOM-10, between 25° and 90° for GOM-11. This pattern suggest that for the GOM-10 with $SSR_x = 0$ a larger portion of applied stress path is close to the near neutral loading. This observation is compatible with the model performance in better simulation of the GOM-11 compared to the GOM-10. For figure-8 type A path, the variation of Θ suggests that the applied stress is predominantly away from the neutral loading. The angle Θ for SANISAND is defined as $\arccos[(\mathbf{n}:\dot{\mathbf{r}})/(\|\mathbf{n}\|\|\dot{\mathbf{r}}\|)]$. In the formulation of SANISAND, the finite size of the yield surface allows for having $\Theta > 90°$ under elastic unloading until stress reversal is detected. The variations of Θ for selected 1-D linear and 2-D linear, circular/oval, and figure-8 type A paths are plotted in Fig. 26 for the first 10 cycles of the loadings. For all of the applied paths, the Θ is always far away from the neutral loading. The oscillations of Θ are also much smaller for SANISAND simulations than for SANICLAY.

This detailed evaluation shows that the SANICLAY formulation can experience the unwanted scenario of proximity to neutral loading condition in certain loading paths, while this does not seem to be the case for SANISAND, at least for the loading paths explored here.

7. Conclusion

Over the years, the SANICLAY and SANISAND models have evolved, and shown very good success in simulating the response in a number of cyclic triaxial tests. These models already possess a number of minimum requirements for their potential application in geotechnical problems involving multidirectional cyclic loading. These requirements include their multiaxial tensorial stress-strain formulation, proper reproduction of soil stiffness and strength, coupling between the volumetric and deviatoric responses, and addressing the changes of soil stiffness in the unloading and reloading sequences.

In multidimensional cyclic shearing, SANICLAY appears to be more successful in capturing the shear strains, while SANISAND is more successful in capturing the pore pressure generation. They both have room for improvement in these complex types of shearing with changing loading directions. In particular, reconsiderations are needed in the coupling of the volumetric and deviatoric responses. SANICLAY appears to underestimate the accumulation of pore pressure

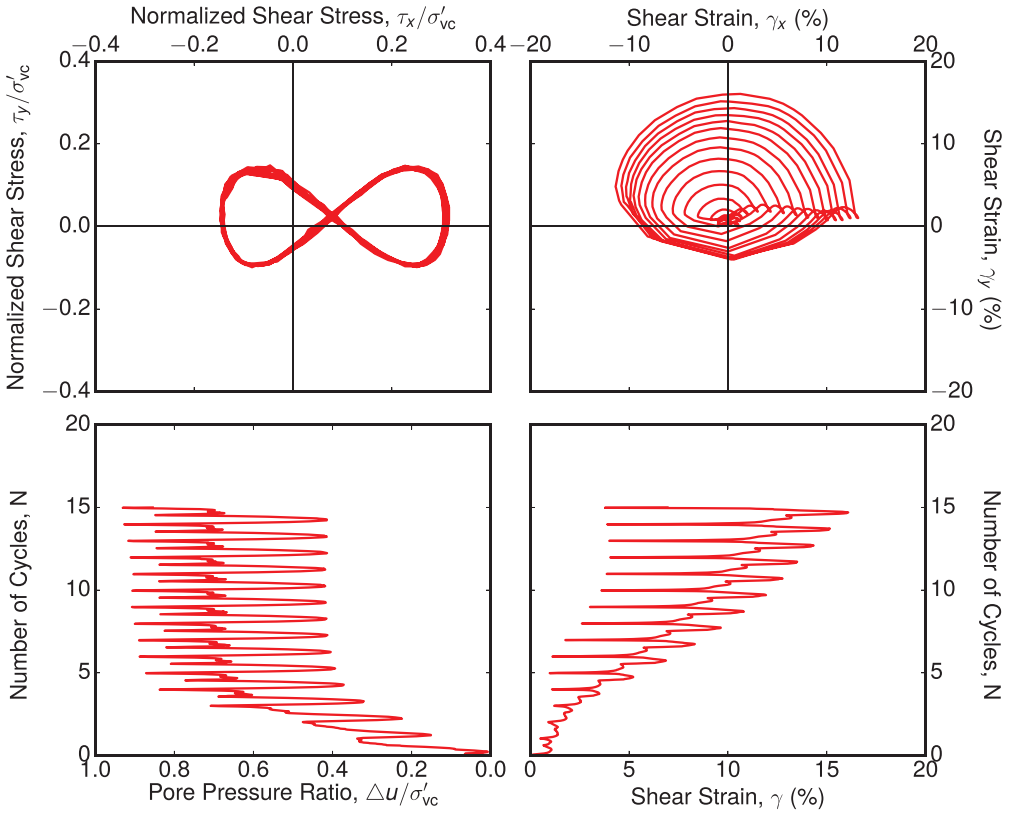

Fig. 22. Simulation versus experiment in figure-8 type A multidirectional cyclic shear test ms38cyck on Monterey No. 0/30 sand: (a) experiment [17] and (b) simulation.

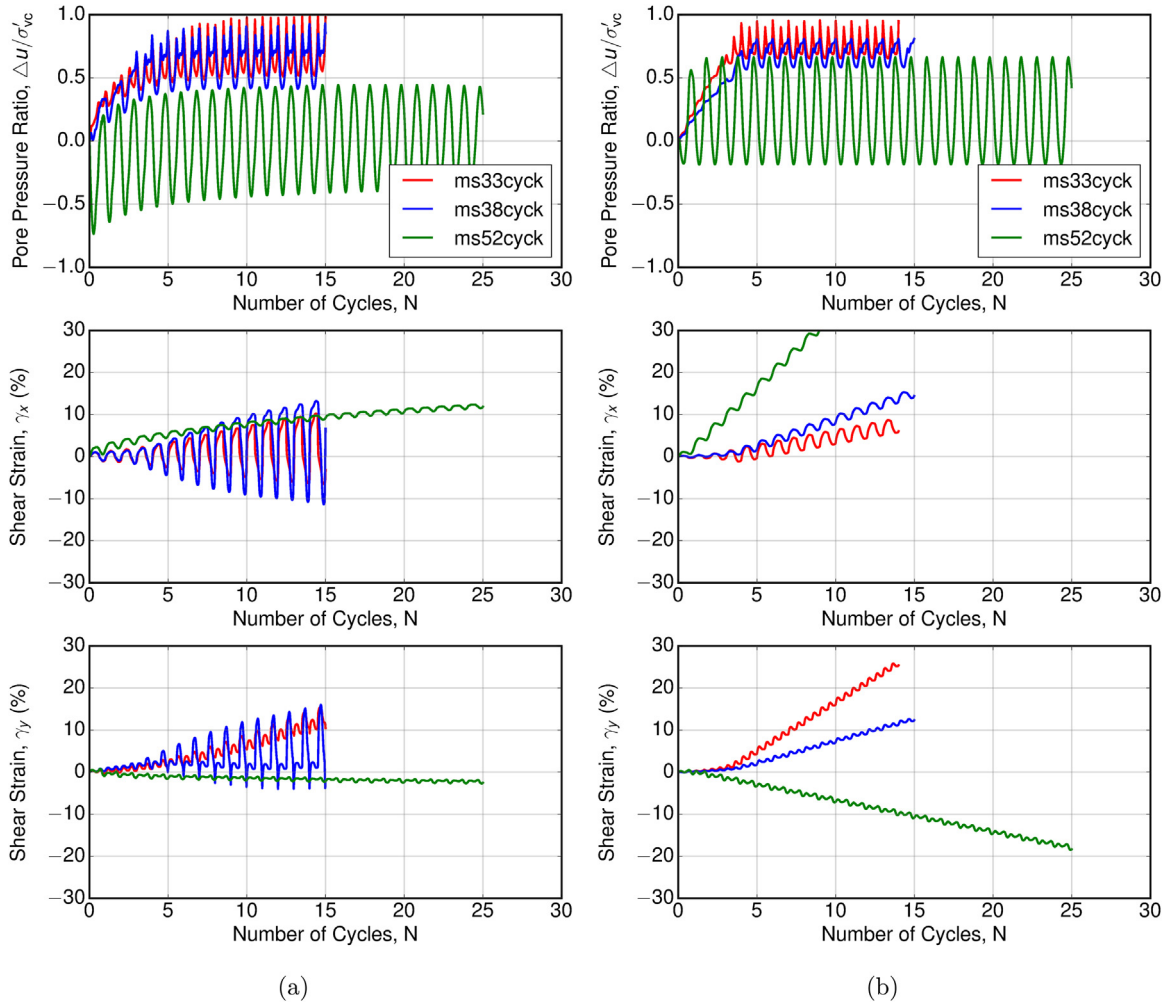

Fig. 23. Simulations versus experiments in figure-8 type A multidirectional cyclic shear tests on Monterey No. 0/30 sand: (a) experiments [17] and (b) simulations.

(volumetric response) in most cases, while accumulation of shear strains (deviatoric response) is simulated much better. SANISAND, however, tends to produce better simulations for pore pressure accumulation (volumetric response) but does not reflect the expansion of shear strains orbit (deviatoric response). In general, both models appear to be less successful for multidirectional cyclic shear tests with $SSR_x \approx 0$, i.e. when initial shear stress is almost absent. One aspect of SANICLAY that needs further investigation is addressing the deficiency of nearly-neutral loading in stress increments nearly tangential to the loading surface. The neutral loading does not seem to be the case for SANISAND, however, the role of fixed and/or evolving fabric tensors and their effects of the deviatoric responses should be further explored in simulations of these complex shearing paths.

In view of the experiments, it must be noted that the assumptions associated with the interpretation of the measured results can potentially mislead the constitutive model evaluations.

Assuming the stress-strain response of laboratory element test as actual representation of soil response under a certain loading at a point, and using that for evaluation of constitutive models would be fair only under uniform distribution of stresses and strains in the laboratory element test. While uniform distribution of these variables is always hypothesized in element tests, it is difficult, if not impossible, to impose idealized boundary conditions that would ensure such uniformity. One of the main deficiency of DSS testing is that complimentary shear stresses on the sides of the specimen cannot be applied and thereby homogeneous stress state cannot be guaranteed. The other limitation is about equalization and uniformity of pore pressures particularly in clay samples subjected to high frequency cycles of loading. Multidirectional shear device inherits these shortcomings from its predecessor DSS device. Although there is a general agreement that with increased specimen diameter to height ratio non-uniformities of stress-strain redistributions is reduced and pore water pressures are more better equalized, these problems cannot be fully eliminated. In addition, different techniques in dealing with specimen could result in different initial fabrics of tested soil.

The multidimensional cyclic shearing is very complex and deserves considerable attention from both laboratory and constitutive modeling perspectives. The success of multidimensional numerical modeling in problems such as earthquake wave propagation, and wind or wave loading of nearshore and offshore structures, is contingent to improvements on testing and modeling of the material response. This is an interesting area of research that is still in early stages of development.

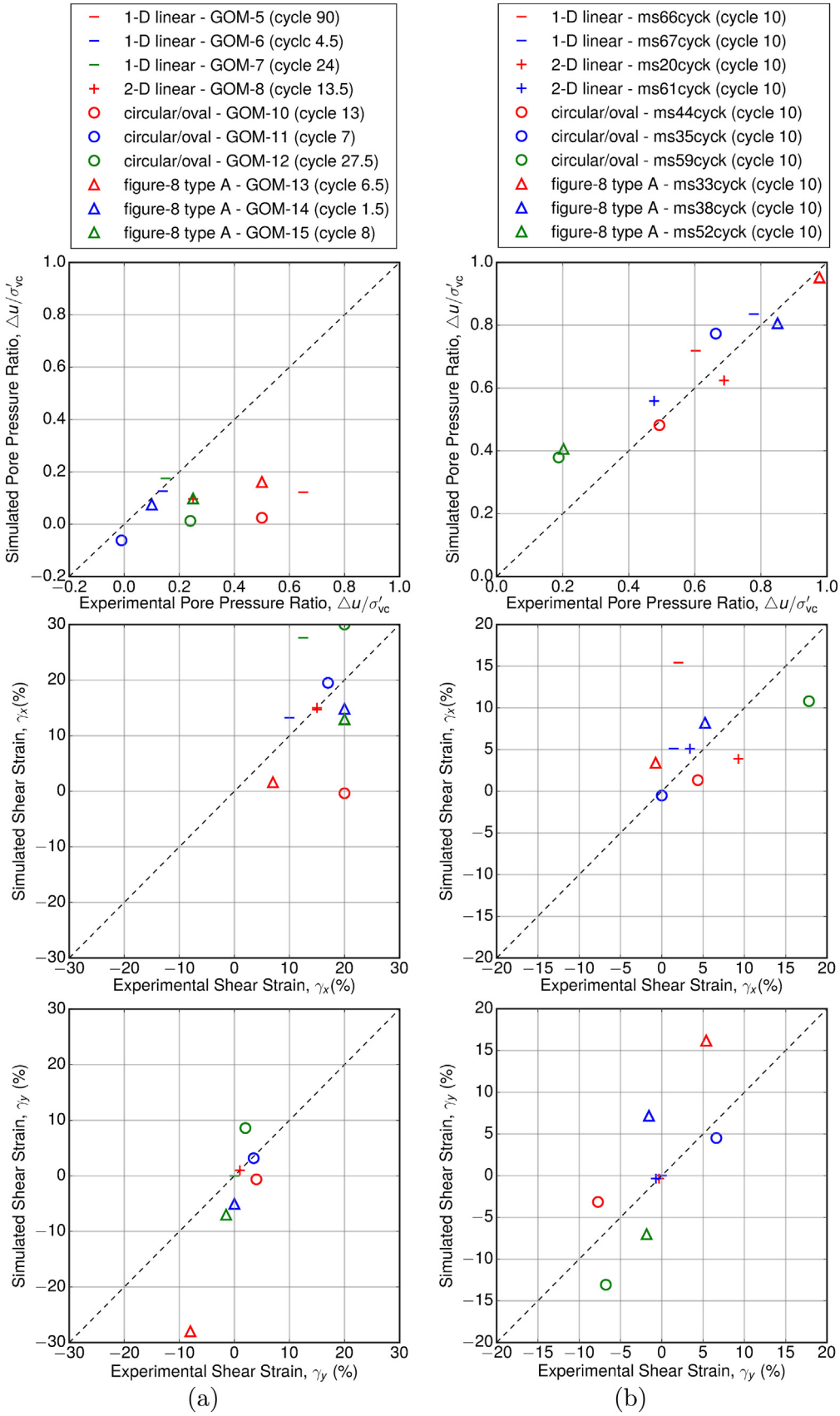

Fig. 24. Simulations versus experiments at the selected points of loading for different types of multidirectional cyclic shear tests on Gulf of Mexico clay (a) and Monterey No. 0/30 sand (b) (Points close to 1:1 line suggests that the corresponding simulation result is close to experiment and vice versa for the points away from 1:1 line).

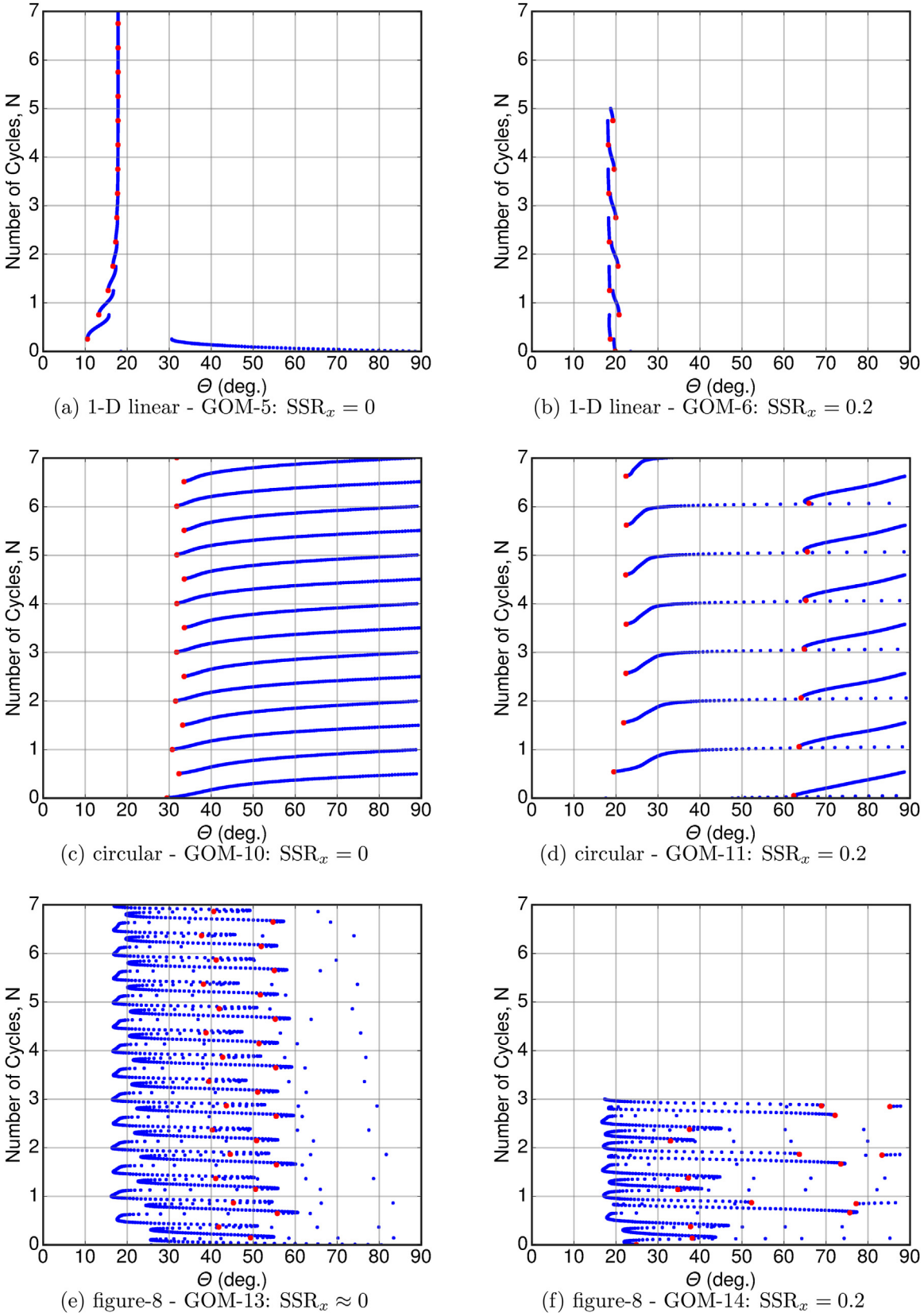

(a) 1-D linear - GOM-5: $\mathrm{SSR}_x = 0$ (b) 1-D linear - GOM-6: $\mathrm{SSR}_x = 0.2$

(c) circular - GOM-10: $\mathrm{SSR}_x = 0$ (d) circular - GOM-11: $\mathrm{SSR}_x = 0.2$

(e) figure-8 - GOM-13: $\mathrm{SSR}_x \approx 0$ (f) figure-8 - GOM-14: $\mathrm{SSR}_x = 0.2$

Fig. 25. SANICLAY: the angle Θ between the gradient of the loading surface ($\partial f/\partial\sigma$) and the stress increment ($\dot{\sigma}$) for cyclic tests simulations. Red circles indicate occurrence of stress reversal during the increment.

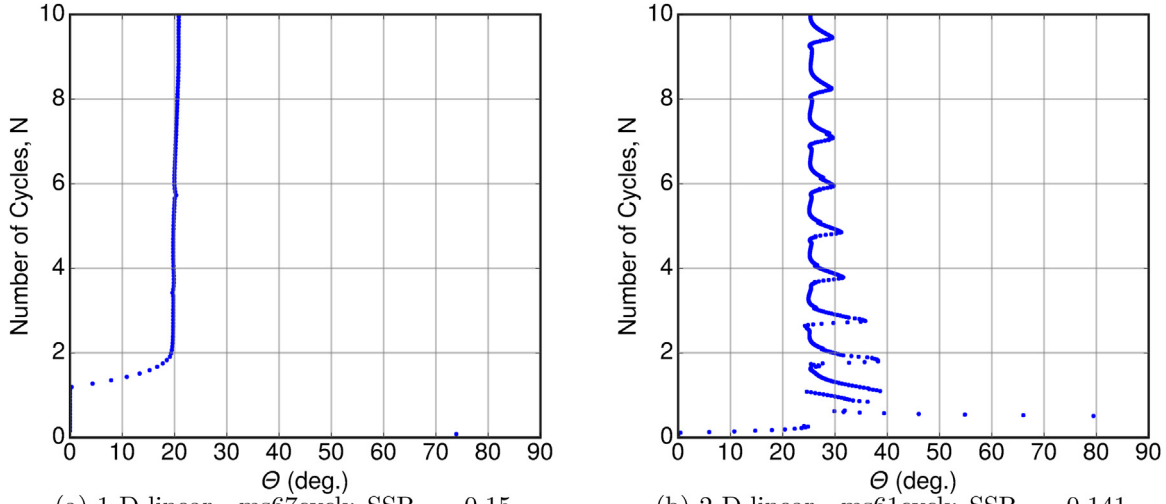

(a) 1-D linear - ms67cyck: $\mathrm{SSR}_x = 0.15$ (b) 2-D linear - ms61cyck: $\mathrm{SSR}_x = 0.141$

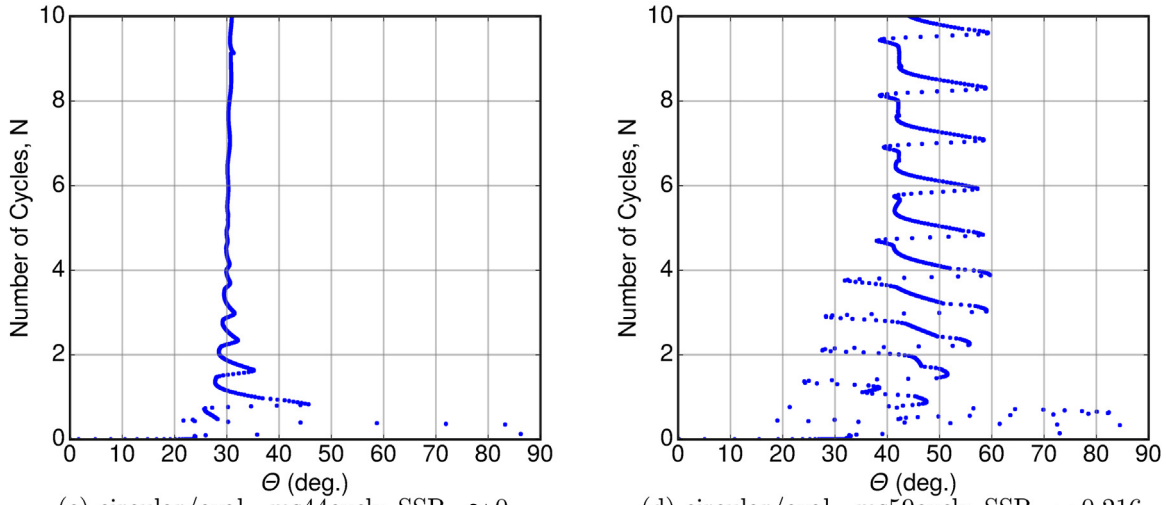

(c) circular/oval - ms44cyck: $\mathrm{SSR}_x \approx 0$ (d) circular/oval - ms59cyck: $\mathrm{SSR}_x = 0.216$

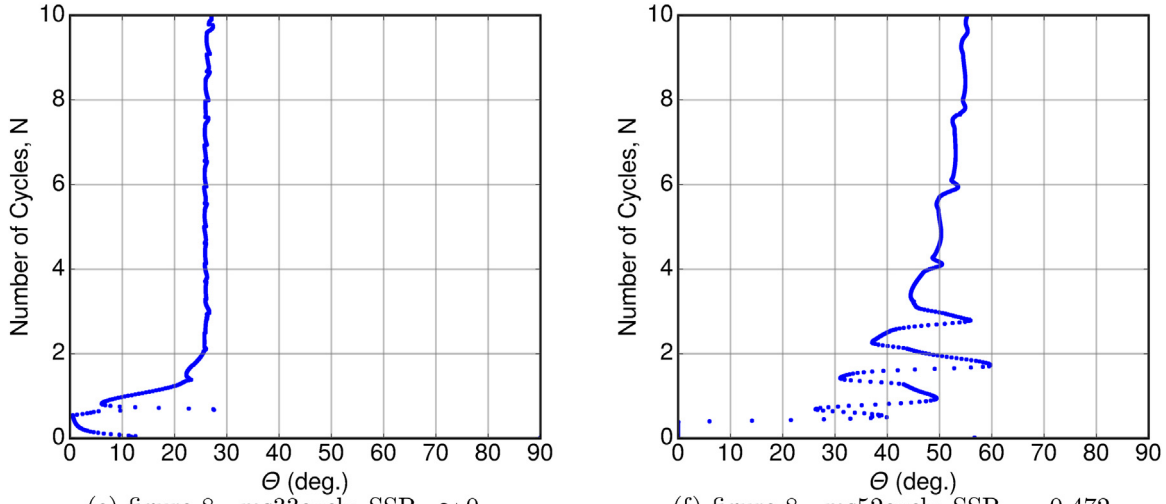

(e) figure-8 - ms33cyck: $\mathrm{SSR}_x \approx 0$ (f) figure-8 - ms52cyck: $\mathrm{SSR}_x = 0.472$

Fig. 26. SANISAND: the angle Θ between the gradient of the yield surface in the stress ratio space ($\mathbf{n}$) and the stress ratio increment ($\dot{\mathbf{r}}$) for cyclic tests simulations.

Acknowledgements

The material presented in this paper is part of an ongoing study at the University of British Columbia on multidirectional modeling in geotechnical seismic analysis and design, with support provided by the Natural Sciences and Engineering Research Council of Canada (NSERC). Stimulating discussions with Professor Yannis Dafalias about the challenges related to the multiaxial constitutive modeling of soils are greatly appreciated.

References

[1] Boulanger RW, Chan CK, Seed HB, Seed RB, Sousa JB. A low-compliance bi-directional cyclic simple shear apparatus. Geotech Test J 1993;16(1):36–45.
[2] Ishihara K, Yamazaki F. Cyclic simple shear tests on saturated sand in multi-directional loading. Jpn SocSoil Mech Found Eng 1980;20(1).
[3] Kammerer AM, Wu J, Riemer MF, Pestana JM, Seed RB. A new multi-directional direct simple shear testing database. In: Proceedings of the 13th World Conference on Earthquake Engineering, 2004, pp. Paper No. 2083, 15 pages.
[4] Matsuda H, Shinozaki H, Okada N, Takamiya K, Shinyama K. Effects of multi-directional cyclic shear on the post-earthquake settlement of ground. In: Proceedings of the thirteenth world conference on earthquake engineering, Vancouver, BC, Canada, 2004, pp. Paper No. 2890, 10 pages.
[5] Duku PM, Stewart JP, Whang DH, Venugopal R. Digitally controlled simple shear apparatus for dynamic soil testing. Geotech Test J 2007;30(5):368–77.
[6] Rutherford CJ, Biscontin G. Development of a multidirectional simple shear testing device. Geotech Test J 2013;36(6):858–66.
[7] Ruldolph C, Grabe J, Albrecht I. Simple shear tests with a varying shearing direction during cyclic shearing. Géotech Lett 2014;4(2):102–7.
[8] Yang Z, Pan K. Flow deformation and cyclic resistance of saturated loose sand considering initial static shear effect. Soil Dyn Earthq Eng 2017;92:68–78.
[9] Ishihara K, Nagase H. Multi-directional irregular loading tests on sand. Soil Dyn Earthq Eng 1988;7(4):201–12.
[10] Matsuda H, Hendrawan AP, Ishikura R, Kawahara S. Effective stress change and post-earthquake settlement properties of granular materials subjected to multi-directional cyclic simple shear. Soils Found 2011;51(5):873–84.
[11] Matsuda H, Nhan TT, Ishikura R. Prediction of excess pore water pressure and post-cyclic settlement on soft clay induced by uni-directional and multi-directional cyclic shears as a function of strain path parameters. Soil Dyn Earthq Eng 2013;49:75–88.
[12] Matsuda H, Nhan TT, Sato H. Estimation of multi-directional cyclic shear-induced pore water pressure on clays with a wide range of plasticity indices. In: Proceedings of the second international conference on civil, structrual and transportation engineering, no. 116, Ottawa, ON, Canada, 2016, pp. 1–8.
[13] Nhan TT, Matsuda H. A development of pore water pressure model for multi-directional cyclic shearing on normally consolidated clays. In: Proceedings of the sixty nineth Canadian geotechnical conference, Vancouver, BC, Canada, 2016, p. 8 pages.
[14] Dyvik R, Berre T, Lacasse S, Raadim B. Comparison of truly undrained and constant volume direct simple shear tests. Geotechnique 1987;37(1):3–10.
[15] Yang M, Taiebat M, Vaid Y. Bidirectional monotonic and cyclic shear testing of soils: state of knowledge. In: Proceedings of the sixty nineth Canadian geotechnical conference, Vancouver, BC, Canada, 2016, pp. Paper ID: 4198, 8 pages.
[16] Boulanger RW, Seed RB, Chan CK, Seed HB, Sousa J. Liquefaction behavior of saturated sands under uni-directional and bi-directional monotonic and cyclic simple shear loading, Geotechnical Engieering Report UCB/GT/91-08, University of California, Berkeley (August 1991).
[17] Kammerer AM, Pestana JM, Seed RB. Undrained response of monterey 0/30 sand under multidirectional cyclic simple shear loading conditions, Geotechnical Engieering Report UCB/GT/02-01, University of California, Berkeley (July 2002).
[18] Rutherford CJ. Development of a multi-directional direct simple shear testing device for characterization of the cyclic shear response of marine clays, Rutherford CJ. Development of a multi-directional direct simple shear testing device for characterization of the cyclic shear response of marine clays, Ph.D. Thesis, Texas A&M University (May 2012).
[19] Nie Y, Fan H, Wang Z, He Z. The influence of cyclic shear direction on static and dynamic characteristics of saturated soft clay. Chin J Rock Mech Eng 2015;34(5):1039–48.
[20] Dafalias YF. An anisotropic critical state soil plasticity model. Mech Res Commun 1986;13(6):341–7.
[21] Dafalias YF, Manzari MT, Papadimitriou AG. Saniclay: simple anisotropic clay plasticity model. Int J Numer Anal Methods Geomech 2006;30(12):1231–57.
[22] Taiebat M, Dafalias YF, Peek R. A destructuration theory and its application to saniclay model. Int J Numer Anal Methods Geomech 2010;34(10):1009–40.
[23] Taiebat M, Dafalias YF, Kaynia AM. Bounding surface model for natural anisotropic clays. in: Papanastasiou P, Papamichos E, Zervos A, Stavropoulou M (Eds.), In: Proceedings of the Ninth HSTAM international congress on mechanics and Vardoulakis mini-symposia, Limassol, Cyprus, 2010, pp. 43–47.
[24] Seidalinov G, Taiebat M. Bounding surface saniclay plasticity model for cyclic clay behavior. Int J Numer Anal Methods Geomech 2014;38(7):702–24.
[25] Papadimitriou A, Vranna A, Dafalias Y, Manzari M. Effect of yield surface shape on the simulated elasto-plastic response of cohesive soils. In: Nordal Benz, editor. Numerical Methods in Geotechnical Engineering. London: Taylor & Francis Group; 2010. p. 63–8.
[26] Dafalias YF, Taiebat M. Anatomy of rotational hardening in clay plasticity. Geotechnique 2013;63(16):1406–18.
[27] Dafalias Y, Taiebat M. Rotational hardening with and without anisotropic fabric at critical state. Geotechnique 2014;64(6):507–11.
[28] Rezania M, Taiebat M, Poletti E. A viscoplastic saniclay model for natural soft soils. Comput Geotech 2016;73:128–41.
[29] Manzari MT, Dafalias YF. A critical state two-surface plasticity model for sands. Géotechnique 1997;47(2):255–72.
[30] Been K, Jefferies MG. A state parameter for sands. Geotechnique 1985;35(2):99–112.
[31] Dafalias YF, Manzari MT. Simple plasticity sand model accounting for fabric change effects. J Eng Mech 2004;130(6):622–34.
[32] Dafalias YF, Papadimitriou AG, Li X-S. Sand plasticity model accounting for inherent fabric anisotropy. J Eng Mech 2004;130(11):1319–33.
[33] Taiebat M, Dafalias YF. Sanisand: simple anisotropic sand plasticity model. Int J Numer Anal Methods Geomech 2008;32(8):915–48.
[34] Li X-S, Dafalias YF. Anisotropic critical state theory: role of fabric. J Eng Mech 2012;138(3):263–75.
[35] Dafalias YF, Taiebat M. Sanisand-z: zero elastic range sand plasticity model. Géotechnique 2016;66(12):999–1013.
[36] Taiebat M, Jeremić B, Dafalias YF, Kaynia AM, Cheng Z. Propagation of seismic waves through liquefied soils. Soil Dyn Earthq Eng 2010;30(4):236–57.
[37] Murali M. Characterization of gulf of mexico clay using automated triaxial testing [Master's thesis]. College Station, TX, USA: Department of Civil Engineering, Texas A&M University; 2011.
[38] Wu J. Liquefaction triggering and post-liquefaction deformation of monterey 0/30 sand under uni-directional cyclic simple shear loading [Ph.D. thesis]. CA, USA: Department of Civil and Environmental Engineering, University of California, Berkeley; 2002.
[39] Seidalinov G. Constitutive and numerical modeling of clay subjected to cyclic loading [Ph.D. thesis]. Vancouver, BC, Canada: Department of Civil Engineering, The University of British Columbia; 2018.
[40] Horita M. Modelling of cyclic behavior of saturated monterey no. 0/30 sand, [Ph.D. thesis]. CO, USA: Department of Civil, Environmental and Architectural Engineering, University of Colorado, Boulder; 1985.
[41] Chen J-W. Stress path effect on static and cyclic behavior of Monterey No. 0/30 sand [Ph.D. thesis]. CO, USA: Department of Civil, Environmental and Architectural Engineering, University of Colorado, Boulder; 1988.
[42] Riemer MF. The effects of testing conditions on the constitutive behavior of loose, saturated sands under monotonic loading [Ph.D. Thesis]. CA, USA: Department of Civil and Environmental Engineering, University of California, Berkeley; 1992.
[43] Liu Y, Sun W, Fish J. Determining material parameters for critical state plasticity models based on multilevel extended digital database. J Appl Mech 2016;83(1):011003.
[44] Taiebat M, Dafalias YF. A zero elastic range hypoplasticity model for sand. Holistic Simulation of Geotechnical Installation Processes. Springer; 2017. p. 237–56.